H4K20me3 controls Ash1-mediated H3K36me3 and transcriptional silencing in facultative heterochromatin

Mareike Möller*, John B. Ridenour[#], Devin F. Wright, Michael Freitag

Department of Biochemistry and Biophysics, Oregon State University, Corvallis OR 97331, USA

[#]Present address: Cell Cycle and Cancer Biology Research Program, Oklahoma Medical Research Foundation, Oklahoma City, OK 73104, USA

*corresponding author: moellmar@oregonstate.edu, mareike.moeller89@gmail.com

keywords: chromatin, facultative heterochromatin, histone methylation, silencing, H4K20

Abstract

Facultative heterochromatin controls development and differentiation in many eukaryotes. In metazoans, plants, and many filamentous fungi, facultative heterochromatin is characterized by transcriptional repression and enrichment with nucleosomes that are trimethylated at histone H3 lysine 27 (H3K27me3). While loss of H3K27me3 results in derepression of transcriptional gene silencing in many species, additional up- and downstream layers of regulation are necessary to mediate control of transcription in chromosome regions enriched with H3K27me3. Here, we investigated the effects of one histone mark on histone H4, namely H4K20me3, in the fungus *Zymoseptoria tritici*, a globally important pathogen of wheat. Deletion of *kmt5*, the gene encoding the sole methyltransferase responsible for H4K20 methylation, resulted in global derepression of transcription, especially in regions of facultative heterochromatin. Reversal of silencing in the absence of H4K20me3 not only affected genes but also a large number of novel, previously undetected, non-coding transcripts generated from regions of facultative heterochromatin on accessory chromosomes. Transcriptional activation in *kmt5* deletion strains was accompanied by a complete loss of Ash1-mediated H3K36me3 and chromatin reorganization affecting H3K27me3 and H3K4me2 distribution in regions of facultative heterochromatin. Strains with a H4K20M mutation in the single histone H4 gene of *Z. tritici* recapitulated these chromatin changes, suggesting that H4K20me3 is essential for Ash1-mediated H3K36me3. The Δ*kmt5* mutants we obtained are more sensitive to genotoxic stressors and both, Δ*kmt5* and Δ*ash1*, showed greatly increased rates of accessory chromosome loss. Taken together, our results provide insights into a novel, and unsuspected, mechanism controlling the assembly and maintenance of facultative heterochromatin.

Significance

Facultative heterochromatin contains genes important for specific developmental or life cycle stages. Transcriptional regulation of these genes is influenced by chromatin structure. Here, we report that a little studied histone modification, trimethylation of lysine 20 on histone H4 (H4K20me3), is enriched in facultative heterochromatin and important for transcriptional repression in these regions in an important agricultural pathogen. Furthermore, normal levels of H4K20me3 are essential for deposition of another repressive histone mark, Ash1-mediated H3K36me3, and affect the distribution of other marks including H3K27me3. We conducted the first genome-wide assessment of H4K20 methylation levels in a fungus, and our discoveries reveal that multiple chromatin modifications are required to establish transcriptional silencing, providing the framework to understand epistasis relationships among these histone marks.

Introduction

Chromatin, the assembly of DNA, RNA, and proteins that constitutes chromosomes, can assume active and inactive states that are correlated with different histone and DNA modifications (1). Transcriptionally inactive, "silent" chromatin is separated into "constitutive heterochromatin", which is most often marked by H3K9me2/3 and DNA methylation and found within or near centromeres, subtelomeric regions or telomere repeats, rDNA, and transposable elements, and "facultative heterochromatin", which is typically enriched with H3K27me3 and found on specific genes (2, 3), in larger BLOCs (broad local enrichments) in mouse (4), or across long sections of chromosomes in many fungi (5, 6). Facultative heterochromatin is more dynamic than constitutive heterochromatin, and "on" or "off" states vary between cell types or individuals within a species (7). While H3K27me3, mediated by Polycomb Repressive Complex 2 (PRC2), is considered to be a hallmark histone modification correlated with facultative heterochromatin (8), little is known about other chromatin marks that are important for formation, maintenance, and gene silencing in these regions. In animals, the PRC1 complex and H2AK119ub1 play an important role in PRC2 and H3K27me3 recruitment (9), but so far there is no evidence for a canonical PRC1-like complex in fungi (10).

Other, less studied, histone modifications found in transcriptionally silent regions of facultative heterochromatin include H4K20 and H3K36 methylation. Depending on the organism, one or multiple histone methyltransferases (HMTs) are responsible for methylating H4K20 (11). In animals, one HMT mediates H4K20me1, for example KMT5A in humans and PR-SET-7 in *Drosophila melanogaster* (12, 13), and at least one additional HMT is responsible for H4K20me2/3, for example KMT5B/C in humans and Su(var)4-20 in *D. melanogaster* (14, 15). In contrast, a single enzyme, Kmt5, called Set9 in *Schizosaccharomyces pombe* and SET-10 in *Neurospora crassa*, catalyzes all H4K20me in fungi (16–18). Presence of the different methylation states of H4K20 (i.e., me1, me2, or me3) are essential for development and associated with DNA repair, replication, cell cycle control, genome stability, and chromatin compaction in animals (11, 19–24). In contrast, there are few studies on fungi addressing the function of H4K20me. In fission yeast, H4K20me is important for DNA repair by recruitment of Crb2 to sites of DNA damage (16). Studies with the filamentous plant pathogenic fungi *Fusarium graminearum*, *F. fujikuroi*, and *Magnaporthe oryzae* (syn. *Pyricularia oryzae*) revealed minor, if any, effects on virulence (17, 18), and only subtle and species-specific effects on expression of secondary metabolite cluster genes and tolerance to stress conditions in Δ*kmt5* strains (17). Surprisingly, none of the previous studies analyzed the genome-wide distribution of any of the H4K20me modification states in fungi.

In contrast, H3K36me is a widespread and well-studied histone modification deposited by Set2 in an RNAPII-dependent manner during transcript elongation (25) and, in some organisms, by another group of RNAPII-independent SET-domain proteins, the ASH1 or NSD family proteins (26, 27). ASH1-mediated H3K36me is linked to Polycomb-mediated repression and is thought to counteract PRC2-mediated H3K27me3 (28, 29). In fungi, ASH1-mediated H3K36me3 co-occurs in regions enriched with H3K27me3 and is important for normal distribution of this mark, at least in *N. crassa* and *F. fujikuroi* (30, 31).

In this study, we wished to address how H4K20me and ASH1-mediated H3K36me3 contribute to the formation, maintenance, and silencing of facultative heterochromatin. The filamentous

89 fungus *Zymoseptoria tritici*, a global pathogen of wheat, has a well-characterized epigenetic
90 landscape, which allowed us to differentiate euchromatin, constitutive or facultative
91 heterochromatin, regions with cytosine methylation (5mC), short regional centromeres,
92 subtelomeric regions, and telomere repeats (6, 32, 33). Facultative heterochromatin, enriched
93 with H3K27me3 and transcriptionally silenced, covers subtelomeric regions and accessory
94 chromosomes (also referred to as "non-essential" or "conditionally dispensable" chromosomes)
95 that create variation between isolates (6, 34). While H3K27me3 in these regions is involved in
96 chromosome stability and accumulation of mutations, loss of H3K27me3 has only minor impacts
97 on transcriptional activation (32, 35). Therefore, we hypothesized that another repressive histone
98 modification exists that is epistatic to H3K27me in *Z. tritici*, and perhaps other organisms.

99 Here we show that H4K20me3 is one such modification and that it is generated exclusively by
100 the SET-domain HMT, Kmt5. Kmt5 and H4K20me3 are crucial for transcriptional silencing in
101 regions of facultative heterochromatin and essential for Ash1-mediated H3K36me3, thereby
102 contributing significantly to formation of H3K27me3-enriched facultative heterochromatin.
103

104 Results

105 Kmt5 and Ash1 are important for normal growth but not essential in *Zymoseptoria*

106 We identified *kmt5* (Zt_chr_3_00475) and *ash1* (Zt_chr_13_00232) in the genome of the reference
107 isolate IPO323 by BLAST searches with *S. pombe* SET9 and *N. crassa* ASH-1 sequences as baits.
108 We found a single H4K20 methyltransferase homolog, consistent with findings in other fungi but
109 different to metazoans, where multiple enzymes are involved in catalyzing H4K20me1 and
110 H4K20me2/3 (Figure 1A). Protein sequence alignments of the SET domains of H4K20
111 methyltransferases in *Z. tritici*, *S. pombe*, *D. melanogaster, Danio rerio*, and human revealed
112 higher sequence similarity between Kmt5 in fungi and known H4K20me2/3 methyltransferases
113 than H4K20me1 methyltransferases (Figure S1). We showed that Kmt5 in *Z. tritici* is responsible
114 for all H4K20 methylation, as *kmt5* deletion strains are unable to generate either H4K20me1 or
115 H4K20me3 (Figures 1B, S2).

116 There is a single gene encoding a *Z. tritici* Ash1 homologue. This Ash1 protein lacks, as does
117 *Neurospora* ASH-1 (30), the C-terminal BROMO, PHD and BAH domains found in animal Ash1
118 homologues but contains the conserved AWS, SET and post-SET domains (Figure 1C). While the
119 specific functions of the additional domains in most animal Ash1 proteins are not known, the
120 PHD and BAH domain are essential for Ash1 to counteract Polycomb-mediated repression in *D.*
121 *melanogaster* (36). Absence of these domains in fungal Ash1 homologs suggests different
122 mechanisms of interaction with chromatin and PRC2, specifically.

123 To determine the function of *kmt5* and *ash1*, we deleted the respective genes in the wild-type
124 isolate Zt09 (37) by replacement with a gene encoding hygromycin phosphotransferase (*hph*),
125 conferring resistance to hygromycin B. Mutant strains were confirmed by PCR and Southern
126 assays (Figure S3). Both deletion mutants exhibit phenotypic differences compared to the wild-
127 type strain. The Δ*kmt5* mutant showed increased sensitivity to genotoxic stress and altered
128 morphology at higher temperatures (28°C *versus* the usual 18°C; Figure 1D). Deletion of *ash1*

129 only slightly retards growth and had overall minor effects on growth under the tested conditions
130 (Figures 1D, S4).
131
132 ## Loss of Kmt5 and Ash1 result in increased chromosome loss
133 Previously, we measured accessory chromosome loss as an indicator for overall genome stability
134 (32). A four-week growth experiment including five replicate cultures of wild-type, Δ*kmt5*, and
135 Δ*ash1* strains revealed an increase in accessory chromosome loss in both mutants (Table 1).
136 Increased chromosome loss rates did not affect all accessory chromosomes equally;
137 chromosomes 14 and 16 in Δ*kmt5*, and chromosome 16 in Δ*ash1* were lost much more frequently
138 than any other accessory chromosomes. This indicates that both Kmt5 and Ash1 are important
139 for the maintenance of at least certain accessory chromosomes, and more likely general genome
140 stability.
141
142 ## ChIP-seq uncovers different heterochromatin states in *Z. tritici*
143 To determine the effects on chromatin in both Δ*kmt5* and Δ*ash1* mutants, we first performed
144 ChIP-seq of selected histone modifications associated with eu- and heterochromatin in wild-type
145 strains. We found that H4K20me3 is widespread along chromosomes, enriched across gene
146 bodies, and exhibits pronounced enrichment in regions we previously characterized as
147 facultative heterochromatin, based on low levels of gene expression and the presence of
148 H3K27me3 (6, 32, 33) (Figures 2A, S5). For the first time, we tested localization of H3K27me2 in
149 *Z. tritici* and found that it is present in the same regions as H3K27me3 but at lower levels of
150 enrichment. H4K20me1 did not show any specific enrichment but was reduced in regions with
151 strong H4K20me3 enrichment, e.g., facultative heterochromatin. H3K36me3 showed a similar
152 pattern and distribution as H4K20me3, and both H3K36me3 and H4K20me3 were absent from
153 constitutive heterochromatin that is marked by H3K9me3 alone, or by a combination of
154 H3K9me3 and H3K27me2/3 (Figures 2A, S5A). To characterize modifications enriched in
155 facultative heterochromatin regions in more detail, we plotted enrichment of H4K20me3 and
156 H3K36me3 within 500 bp windows of regions that are enriched with H3K27me3 in wild type
157 (Figure 2B). We found two distinct clusters within H3K27me3-enriched regions: cluster 1 was
158 enriched with H4K20me3 and H3K36me3, while cluster 2 exhibited very low levels of H3K36me3
159 and H4K20me3. Further analyses of the genomic context of these clusters revealed that cluster
160 1 mostly overlaps with genes and intergenic regions, while cluster 2 overlaps with transposable
161 elements (TEs) that are also enriched with H3K9me3, few genes, and intergenic regions (Figure
162 2C). H3K27me3 and H3K9me3 co-occur in regions close to the telomeres, some repeats, and
163 sections of accessory chromosomes; the common feature of these regions are TEs. Both
164 H3K36me3 and H4K20me3 are predominantly excluded from these regions.

165 These two clusters may signify functionally different types of facultative heterochromatin, with
166 cluster 1 representing the traditionally accepted type of facultative heterochromatin
167 conditionally repressing genes, while cluster 2 represents constitutive heterochromatin doubly
168 marked with H3K9me3 and H3K27me3. Based on these results we now differentiate at least
169 three types of heterochromatin in *Z. tritici*: (1) constitutive heterochromatin, correlated with
170 H3K9me3 enrichment only and enriched on repeats and TEs, (2) constitutive heterochromatin,

171 correlated with enrichment of H3K9me3 and H3K27me3, found close to telomeres and some
172 repeats and TEs, especially on accessory chromosomes, and (3) facultative heterochromatin,
173 correlated with H3K27me3, H3K36me3, and H4K20me3 enrichment, mostly found on genes and
174 intergenic regions either in large blocks or in shorter segments dispersed on chromosomes. The
175 functional relevance of these states remained to be determined and here we began these
176 investigations.
177

178 Facultative heterochromatin marked by H4K20me3, H3K36me3, and H3K27me3 shows 179 strong interactions

180 To further characterize chromatin states and their influence on spatial interactions in the nucleus,
181 we performed Hi-C experiments to find regions in the genome that physically interact. We
182 compared wild type and a Δ*kmt6* mutant to see if loss of H3K27me3, the hallmark modification
183 of facultative heterochromatin, impacts interaction frequencies in specific regions. We found
184 strong interactions between regions enriched with H3K27me3 that we characterized as
185 facultative heterochromatin (cluster 1) in wild type (Figure 3). As in other organisms (38–41)
186 centromeres, which cannot be identified by a single chromatin mark in *Z. tritici* (6), interact most
187 strongly. Large blocks of facultative heterochromatin are found on accessory chromosomes and
188 on the right arm of chromosome 7. These blocks show strong inter- and intrachromosomal
189 interactions but few interactions with non-facultative heterochromatin regions (Figure 3),
190 revealing that they are physically separated from euchromatin. When comparing results from
191 wild type to those from the Δ*kmt6* mutant, we found that these strong interactions between
192 facultative heterochromatin regions persist, even in absence of H3K27me3 indicating that other
193 mechanisms and not H3K27me3 alone are responsible for these strong interactions. Notably,
194 H4K20me3 enrichment was not affected by absence of H3K27me3 in the Δ*kmt6* mutant (Figures
195 3B, S6).
196

197 Kmt5 is essential for Ash1-mediated catalysis of H3K36me3 and normal H3K27me3 198 distribution

199 Deletion of *kmt5* resulted in complete loss of H4K20me3 (Figures 1B and 4) and impacted the
200 distribution of several other histone modifications tested (Figures 4 and S7, S8). Most
201 prominently, we found that H3K36me3 was lost from most regions in which it co-localized with
202 H3K27me3 in wild type. The same regions lost H3K36me3 in the *ash1* deletion mutant, indicating
203 that Ash1 activity is compromised in the *kmt5* mutant. Loss of Ash1, however, does not impact
204 H4K20me3, indicating that H4K20me3 is epistatic to, or acts upstream of, Ash1-mediated
205 H3K36me3.

206 While impacts on H3K36me3 were similar in *kmt5* or *ash1* deletion strains, loss of *kmt5* had more
207 severe effects on H3K27me3 enrichment. In the absence of Kmt5, we observed major changes
208 in H3K27me3 distribution, including losses of large blocks of H3K27me3, some movement to
209 constitutive heterochromatin, and losses and gains of peaks in numerous shorter dispersed
210 peaks. In addition, loss of H4K20me3, H3K36me3, and H3K27me3 in the Δ*kmt5* mutant was
211 often accompanied by gain of H3K4me2, suggesting a transition from facultative
212 heterochromatin to transcriptionally active euchromatin (Figure 4A). In contrast, we detected

fewer differences in H3K27me3 enrichment in the *ash1* mutant, mostly losses or gains in a limited number of the shorter dispersed peaks and increased enrichment in large H3K27me3-enriched blocks on accessory chromosomes.

We found that most changes in chromatin states in Δ*kmt5* and Δ*ash1* mutants occurred in regions that we characterized as facultative heterochromatin (cluster 1), i.e., regions that show enrichment for H3K27me3, H3K36me3, and H4K20me3, but to a much lesser extent in regions outside of facultative heterochromatin (Figure S7). Looking specifically at enrichment of the three marks in those regions in wild type and mutants (Figure 4B), we found that, as expected, H4K20me3 is absent in Δ*kmt5* but only slightly reduced in Δ*ash1*. H3K27me3 was reduced in many regions in Δ*kmt5* but slightly increased in Δ*ash1*, and H3K36me3 was greatly reduced in Δ*ash1* and only slightly less so in Δ*kmt5* when compared to enrichment in wild type. Taken together, we showed that Kmt5 is important for facultative heterochromatin assembly and maintenance and that it is essential for Ash1 activity.

H4K20M mutation alters abundance and distribution of H4K20me3

To test whether the presence of the Kmt5 protein or its catalytic activity, i.e., methylation of H4K20, is important for H3K36me3, we constructed histone H4K20 mutants, replacing lysine residue 20 with a methionine. We generated two different types of mutants, one a clean replacement of the single endogenous histone H4 gene (*hH4*) by $hH4^{K20M}$ ($H4^{K20M}$) and the second an ectopic addition of $hH4^{K20M}$, generating the potential for a mixed population of nucleosomes ($H4^{K20/K20M}$). The replacement allele recapitulated results obtained with the Δ*kmt5* mutant, showing complete absence of H4K20me3, loss of Ash1-mediated H3K36me3, and reduced H3K27me3 enrichment, revealing that presence of the histone mark, but not necessarily presence of the Kmt5 protein, is essential for Ash1 recruitment (Figures 5A-C, S8). In contrast, we observed striking differences in H4K20me3 distribution in the strain with the ectopic $hH4^{K20M}$ integration ($H4^{K20/K20M}$). In this mutant, H4K20me3 enrichment was retained only in specific regions, co-localizing with Ash1-mediated H3K36me3 and H3K27me3 but lacking from the rest of the genome. Analysis of the regions enriched with H4K20me3 in the $hH4^{K20/K20M}$ mutant revealed that H3K36me3 was still slightly reduced compared to wild type, but levels were higher than in both Δ*kmt5* and $hH4^{K20M}$ mutants, while H3K27me3 enrichment was comparable to wild type (Figure 5A-C). Presence of H4K20me3 in these regions suggests that these regions are preferential targets of Kmt5. Based on data collected with mutant histone H4 alleles, presence of H4K20me3 appears to be necessary to deposit H3K36me3 and H3K27me3 and thus for maintenance of a facultative heterochromatin state.

Tagging of Kmt5 impairs protein function and limits H4K20me3 spreading

In order to characterize Kmt5 in more detail, we generated strains harboring N-terminally (*V5-gfp-kmt5*) or C-terminally (*kmt5-gfp-3xFLAG*) tagged Kmt5 alleles by either replacing the endogenous *kmt5* in wild type or complementing the Δ*kmt5* mutant at the original locus. Based on ChIP-seq analyses, none of these mutants retained or restored wild-type levels of H4K20me3 enrichment. H4K20me3 levels were similar to those observed in the $H4^{K20/K20M}$ strain in specific locations co-localizing with Ash1-mediated H3K36me3 and H3K27me3 but mostly absent from

255 the rest of the genome (Figure 5D). The C-terminally tagged Kmt5 mutant maintained some
256 H4K20me3 outside of facultative heterochromatin but not at levels comparable to those in wild
257 type.

258 Notably, integration of the C-terminally tagged Kmt5 in either wild-type or Δ*kmt5* backgrounds
259 led to similar defects in H4K20me3 distribution. This suggests the difference in H4K20me3 is not
260 a result of impaired *de novo* deposition of H4K20me3 after complete loss of the modification
261 but rather a defect in H4K20me3 genome-wide deposition or maintenance associated with
262 impaired function of the tagged Kmt5 protein (Figure S8).
263

264 ## Eaf3 is essential for Ash1 activity

265 To further investigate the connection between H4K20me3 and H3K36me3, we searched the
266 genome for predicted proteins that, in other organisms, have been shown to bind to H4K20me3
267 or to interact with either Ash1 or Kmt5. In *S. pombe*, a PWWP domain-containing protein (Pdp1)
268 occurs in a complex with Kmt5 and is required for all H4K20me (42). We found a single protein
269 with a PWWP domain in *Z. tritici* (Zt_chr_4_873) and other filamentous fungi (Figure 6A). Deletion
270 of the respective gene in *Z. tritici* did not affect H4K20me3 or H3K36me3 (Figure 6B and C) but
271 rather led to increased enrichment of H3K27me3 in numerous regions along the genome
272 (Figures S7, S8, S9), suggesting that there is no homolog of the *S. pombe* Pdp1 in filamentous
273 fungi but that this protein is important for regulation of other chromatin states. A homolog of *Z.*
274 *tritici* Pdp1 was found to interact with a chromatin remodeling factor, ISWI, in *N. crassa*, where it
275 also increased H3K27me3 levels; thus *Z. tritici* Pdp1 is a putative homolog of *S. cerevisiae* Ioc4
276 (43).

277 Our second candidate protein for connecting H4K20 methylation and Ash1 is a homolog of the
278 chromodomain-containing protein Eaf3 in *S. cerevisiae* or MRG15 in *D. melanogaster*. In yeast,
279 Eaf3 is part of the histone deacetylase complex Rpd3S (44) and the histone acetyltransferase
280 complex NuA4 (45), and its chromodomain can bind to both H3K36me3 and H4K20me3 *in vitro*
281 (46), though not at the same time. *Drosophila* MRG15 interacts with Ash1 and is essential for
282 Ash1 function (47). We deleted the *Z. tritici* homolog of the *eaf3* gene (Zt_chr_1_1455) and
283 performed ChIP-seq on the mutant. Absence of *eaf3* resulted in loss of H3K36me3 in the same
284 regions where we observed loss of H3K36me3 in Δ*ash1* and Δ*kmt5* mutants indicating that Eaf3
285 is required for Ash1 activity (Figures 6B and C, S7, S8). Eaf3 was not required for H4K20me3; on
286 the contrary, we observed increased levels of H4K20me3 in the Δ*eaf3* mutant in regions that are
287 targeted by Ash1 in wild type (Figure 6B and C). We did not observe a similar increase outside
288 of regions of facultative heterochromatin. Because we did not detect a similar increase in
289 H4K20me3 in Δ*ash1* mutants, it is not absence of H3K36me3 but a mechanism upstream of Ash1
290 recruitment that influences H4K20me3 levels in Δ*eaf3*.
291

292 ## A Rad23 homolog may act as a histone H4K20me3 demethylase

293 A recent study found that two human hHR23 proteins, homologs of *S. cerevisiae* Rad23, act as
294 demethylases of H4K20me1/2/3 in human cells (48). We found one potential homolog of yeast
295 Rad23 in *Z. tritici* (previously not annotated, on chr 2: 3,656,371-3,657,715) and deleted the
296 putative *rad23* gene to determine whether Rad23 is involved in H4K20me3 demethylation in *Z.*

297 *tritici*. We found increased levels of H4K20me3 in facultative heterochromatin in Δ*rad23* strains
298 and minor differences in H4K20me3 levels outside of these regions indicating that Rad23 may
299 be involved in demethylation of H4K20, particularly in facultative heterochromatin regions
300 (Figure 6B and C, S7, S8).
301

302 ## H4K20me is required for transcriptional repression in facultative heterochromatin

303 To investigate whether the observed changes in chromatin structure correlate to changes in gene
304 expression, we sequenced mRNA from three replicates of wild type, Δ*kmt5*, Δ*ash1*, Δ*eaf3*,
305 *hH4*^{K20M}, and *hH4*$^{K20/K20M}$ strains and determined which genes were differentially expressed
306 (Figures 7A, S10). As a control for the H4$^{K20/K20M}$ strain, we also included a strain that carries an
307 ectopic wild-type H4 copy. We detected few (only 10) differentially expressed genes between
308 wild type and this strain, concluding that an additional wild-type H4 copy has negligible impact
309 under these conditions (Table S1). We showed previously (32) that loss of H3K27me3 alone has
310 surprisingly minor effects on transcription, as only a few genes, mostly located on accessory
311 chromosomes, showed increased levels of expression. In contrast, deletion of *kmt5* results in
312 upregulation of a large set of genes, especially in regions of facultative heterochromatin that are
313 usually enriched with H3K27me3, Ash1-mediated H3K36me3, and H4K20me3. Out of 718
314 upregulated genes ($\log_2$fc >| 0.585 |, padj <0.01, Figure 7A) in Δ*kmt5*, 286 are located in
315 facultative heterochromatin (~40% of upregulated genes). Similarly, 39% of upregulated genes
316 in *hH4*^{K20M} are within facultative heterochromatin, indicating that Kmt5 and H4K20me3 are
317 especially important for gene repression in those regions. While we also observed upregulation
318 of genes in facultative heterochromatin in the other mutants, their relative proportion is
319 considerably lower (26% in Δ*ash1*, 19% in *hH4*$^{K20/K20M}$, and 15% in Δ*eaf3*). H4K20me3 levels in
320 these mutants were largely unchanged or even increased (Δ*eaf3*) suggesting that presence of
321 H4K20me3 may limit derepression. We found that more than 55% of upregulated genes were
322 shared in Δ*kmt5* and Δ*ash1* mutants and almost 90% of upregulated genes in the *hH4*^{K20M} mutant
323 were also upregulated in Δ*kmt5*, Δ*ash1*, or both. In general, a large proportion of upregulated
324 genes are shared in the mutants we sequenced, indicating that they affect a common silencing
325 pathway (Figure S10). Most of the upregulated genes (~94%), as well as genes in facultative
326 heterochromatin in general, lack functional annotations (only 57 out of 976 [~6%] genes have
327 been previously annotated in these regions), making it difficult to assess enrichment for putative
328 functions among those genes. A list including all genes, expression levels, and predicted function
329 can be found in Table S1.

330 We noticed that, especially on accessory chromosomes, many regions without previously
331 annotated genes or with incorrectly annotated genes showed transcriptional activity, often in a
332 strand-specific manner and generating spliced transcripts, suggesting typical fungal transcription
333 to generate mRNA by RNAPII. Many of these transcripts were more highly or newly expressed in
334 the Δ*kmt5* mutant. To quantify the number of new transcripts that were not captured by the
335 current gene annotation, we used stringtie (49) to identify transcripts in the combined RNA-seq
336 data of all strains. We identified a total of 1,023 transcripts in facultative heterochromatin, of
337 which only 516 were partially or fully overlapping with the previous annotation. Expression levels
338 of these transcripts were highest in Δ*kmt5* and *hH4*^{K20M} followed by Δ*ash1* (Figure 7B). The Δ*eaf3*

339 and *hH4*$^{K20/K20M}$ strains exhibited only slightly higher expression of these transcripts (Figure 7B).
340 Many of the newly discovered transcripts do not appear to encode for proteins, as they contain
341 numerous, presumably premature, stop codons in all three reading frames. To better understand
342 the potential function of these transcripts, we manually annotated all transcripts expressed on
343 one accessory chromosome (chromosome 17), their chromatin state (in wild type), presence of
344 additional copies of homologs on other accessory or core chromosomes, any potential function
345 based on blastx searches, and presence of homologs in other species (Tables 2 and S2). We
346 identified a total of 186 transcripts of which 55 match or partially match the previous annotation.
347 Only 13 of these 186 transcripts seem likely to encode a protein based on the presence of an
348 open reading frame without premature stop codons; one of these transcripts encodes a putative
349 protease, while the others showed no predicted functional domains. If these 186 transcripts do
350 not encode proteins, they may function as regulatory RNAs. We looked for homologous genes
351 or sequences on other accessory chromosomes or core chromosomes using blastn searches in
352 the *Z. tritici* wild-type genome. Almost half of the transcripts (89/186) on chromosome 17 had
353 copies on other accessory chromosomes, often multiple copies on multiple chromosomes.
354 Almost one third (62/186) showed similarity to sequences or genes on core chromosomes.
355 Among the homologs on core chromosomes and functional annotation based on blastx searches,
356 we found a striking enrichment of genes that encode for proteins involved in chromosome
357 organization and segregation and cell cycle control. For example, we found eleven transcripts
358 with similarity to the gene encoding a Shugoshin homolog (chr12_379), a protein that is
359 important for chromosome cohesion during mitosis and meiosis. Seven transcripts are similar to
360 those for protein kinases that are important for cell cycle control, one transcript has homology
361 to transcripts of the kinetochore subunit, CenpC, two transcripts are similar to those of alpha
362 tubulin, two transcripts are similar to those of two different Snf2 chromatin remodeling ATPases,
363 and one transcript is similar to Sir2 histone deacetylase transcripts (Table S2). Half of these
364 conserved transcripts are expressed as antisense mRNAs to the transcripts produced from their
365 core chromosome homolog, while the other half is expressed from the same strand. Homologous
366 genes on core chromosomes were not differentially expressed in any of the mutants, except for
367 four genes (three in Δ*eaf3* and one in *hH4*^{K20M}), but these do not seem to correlate with
368 corresponding transcript expression levels on chromosome 17.
369

370 Discussion

371 We report chromatin dynamics and interactions in facultative heterochromatin that identify Kmt5
372 and H4K20me3 as important regulators for transcriptional repression and recruitment of Ash1-
373 mediated H3K36me3, which itself at least partially regulates the distribution of H3K27me3. Here
374 we investigated potential epistasis rules for repressive histone modifications and show that
375 presence of H4K20me3 and Kmt5 are essential for Ash1-mediated H3K36me3, because we
376 observed absence of H3K36me3 in selected regions upon either deletion of Kmt5 or introduction
377 of a mutant histone H4^{K20M}. We determined that H3K27me3 is controlled by both H4K20me3
378 and H3K36me3 levels, at least in most regions with H3K27me3 enrichment. Previously, no
379 genetic or physical interactions between H3K36me3 and H4K20me3, or the methyltransferases

380 involved (Ash1 and Kmt5, respectively) had been described. Our findings suggest that H4K20
381 methylation needs to be established before Ash1 can catalyze H3K36me3.

382 Based on our ChIP-seq, H4K20me3 is a widespread mark, heavily enriched along *Z. tritici*
383 chromosomes, especially in regions that are enriched with H3K27me3, segments of the genome
384 we refer to as facultative heterochromatin. Here we elucidated the function of H4K20me3 in the
385 formation and maintenance of facultative heterochromatin. Why H4K20me3 is also enriched
386 across some gene bodies outside of facultative heterochromatin remains unclear. In fungi, Kmt5
387 catalyzes all three methylation states, which makes it difficult to disentangle the relative
388 importance of the three different potential H4K20 methylation states. By ChIP, we showed that
389 H4K20me1 is not specifically enriched along the genome, but we showed that levels are lower
390 in facultative heterochromatin, where H4K20me3 enrichment is highest, suggesting that these
391 two methylation states do not coexist in facultative heterochromatin under the tested conditions.
392 This makes the trimethyl state the most likely to be responsible for the effects we observed in
393 facultative heterochromatin. We currently have no data on the distribution of H4K20me2.

394 In animals, H4K20 methylation is found in various chromatin environments, and in a tissue- and
395 life stage-dependent manner (11). Because of the presence of multiple H4K20
396 methyltransferases, non-histone targets, and interdependency of methylation states, distinct
397 roles for the different methylation states are difficult to study. H4K20me1 has been associated
398 with both active (24, 51), as well as repressed genes (52), promoting chromatin openness (24),
399 but is also enriched in inactive regions, such as the inactivated X-chromosome (53). Previous
400 studies found that H4K20me3 levels increase during senescence and aged tissues but decrease
401 in cancer cells, which is associated with both increased and decreased silencing, respectively,
402 suggesting that H4K20me3 is important in suppressing tumorigenicity (54, 55). The C-terminus
403 of KMT5C has been shown to interact with HP1, targeting H4K20me3 to H3K9me3-enriched
404 regions, such as TEs, telomeres and pericentric regions (56, 57). This overlap of H4K20me3 with
405 H3K9me3 is completely absent from *Z. tritici*, suggesting that Kmt5 has different interaction
406 partners than in animals: H4K20me3 is not involved in silencing of constitutive heterochromatin
407 in this species. In contrast to animals, fungi only possess a single methyltransferase mediating all
408 H4K20me, as opposed to different enzymes catalyzing either H4K20me1 or H4K20me2/3. The
409 presence of different H4K20 HMTs may result in more specialized interactions with different
410 complexes that are specific to the different states of H4K20 methylation.

411 We found that H4K20me3 overlaps with Ash1-mediated H3K36me3 and H3K27me3 in
412 facultative heterochromatin but also co-occurs with H3K36me3 outside of these regions. An
413 overlap of H4K20me3 and H3K36me3 in gene bodies of actively transcribed genes has been
414 shown in embryonic stem cells, possibly resembling the mechanisms that are responsible for
415 H4K20me3 enrichment outside of facultative heterochromatin regions we found here (58). Very
416 little is currently known about the connection between H4K20me and H3K27me3. H4K20me3
417 and H3K27me3 have been shown to co-occur on some transposons in *Xenopus tropicalis*
418 embryos (59) and a similar recruitment mechanisms to X-chromosomes has been proposed for
419 H4K20me1 and H3K27me3 (53). Results from other fungi are sparse, as no genome-wide studies
420 have been carried out, even in model organisms such as *S. pombe* and *N. crassa*. Lastly, H4K20

421 methylation appears to be lacking completely in plants (60), suggesting that the control of
422 H3K27me3-mediated facultative heterochromatin is regulated in entirely different ways.

423 To understand the biochemistry of a putative Kmt5 complex, we tagged the protein with GFP
424 and short tags for protein purification. We showed that both N- and C-terminal tags greatly
425 interfered with normal Kmt5 function, as documented by ChIP-seq. Taken together with our
426 results on the added histone $H4^{K20M}$ allele ($H4^{K20/K20M}$), facultative heterochromatin may be the
427 first region in which H4K20 methylation occurs, and from which this histone mark spreads into
428 the bulk of the chromatin to normal levels observed in wild type. It is unclear how this partial
429 activity occurs, but studies on other histone mutants, specifically $H3^{K27M}$ showed that K to M
430 mutations alter the release of histone methyltransferases from their substrates and thus sequester
431 them on chromatin (61, 62). The consequence is limited or greatly reduced activity of the
432 methyltransferase in other parts of the genome, which is what we observed with the $H4^{K20/K20M}$
433 mutant. The reason N- and C-terminal Kmt5 fusion proteins show similar distribution may well
434 relate to the overall structure of the Kmt5 protein, with the N-terminus being slightly more
435 sensitive to modifications or additions than the C-terminus. In the absence of fully, or at least
436 largely, complementing tagged alleles of Kmt5 we will address Kmt5 biochemistry in a separate
437 study.

438 How then does H4K20 trimethylation govern facultative heterochromatin *de novo* assembly and
439 maintenance? Our current working model (Figure 8) proposes that in maintenance mode either
440 Kmt5 alone, or in a complex, methylates H4K20 in regions that are already enriched with
441 methylated H4K20. For *de novo* methylation, some "signal" must be present. When Kmt5 is
442 reintroduced into a Δ*kmt5* mutant, the protein, alone or in a complex, is able to detect such
443 signals and methylate H4K20, as observed in the tagged Kmt5 strains we generated. These
444 signals do not appear to be other histone modifications we analyzed in this study (H3K27me3,
445 Ash1-mediated H3K36me3), as none of the mutants, except for Δ*kmt5* and histone *H4* mutants,
446 reduced H4K20me3 levels in facultative heterochromatin. Analyses of putative DNA-based
447 sequence motifs in regions enriched with H4K20me3 in the $H4^{K20/K20M}$ mutant did not yield
448 candidates.

449 Independently from how Kmt5 first finds its targets, it seems likely that H4K20me3 is bound by
450 Eaf3 which then stimulates activity of Ash1, as shown for MRG15 in flies (47, 63); this is supported
451 by finding increased H4K20me3 levels in the absence of Eaf3 and the requirement of Eaf3 for
452 Ash1-mediated H3K36me3. Whether Eaf3 is part of an Rpd3S-like complex in filamentous fungi,
453 or whether it may directly recruit Ash1 to regions of H4K20me3 remains unknown. We propose
454 that Ash-1-mediated H3K36 methylation results in a switch of Eaf3 binding from H4K20me3 to
455 H3K36me3, though it is also possible that it may bind both modifications at the same time.

456 Little is known about proteins that interact with Kmt5 in fungi except for *S. pombe* Pdp1 (42).
457 Here we showed that there is no true ortholog for this protein in filamentous fungi, and that the
458 best homolog in *Z. tritici* and other filamentous fungi is an ortholog of PWWP domain *S.*
459 *cerevisiae* loc4 protein, a component of some ISWI chromatin remodeling complexes in *N. crassa*
460 (43). While this protein does not seem to be important for H4K20me3, we did observe increased
461 enrichment of H3K27me3 outside of wild-type facultative heterochromatin regions, suggesting

462 an important role in chromatin regulation; modest increases of H3K27me3 enrichment was also
463 observed in *N. crassa* (43).

464 Similar to findings in *N. crassa* and *F. fujikuroi* but unlike in animals, H3K27me3 and Ash1-
465 mediated H3K36me3 occur in the same regions (28, 30, 31, 36). Loss of Ash1-mediated
466 H3K36me3 has minor impacts on H3K27me3 in *Z. tritici*, resulting in increased enrichment in
467 some regions and decrease in other regions. While Ash1 in animals is predominantly a
468 H3K36me2 methyltransferase, we found major impacts on H3K36me3, as shown previously in *N.*
469 *crassa* and *F. fujikuroi* (30, 31). The fungal Ash1 proteins are different from Ash1 in animals, as
470 they lack the C-terminal Bromo, PHD and BAH domains, suggesting they have different
471 chromatin binding properties and thus functions than their animal homologs.

472 Functional analyses of the Kmt5 homolog in *S. pombe*, Set9, and some of the animal Kmt5
473 proteins suggest importance during replication and DNA repair (15, 16, 20, 21, 64, 65). Here we
474 showed that both Kmt5 and Ash1 are necessary, but not essential, for normal growth of *Z. tritici.*
475 While the Δ*ash1* mutant showed only minor effects under our conditions, the Δ*kmt5* mutant was
476 more sensitive to genotoxic stress, especially at higher temperatures. Lack of both Kmt5 and
477 Ash1 also resulted in accelerated chromosome loss rates: While the loss rate for wild type was
478 ~3%, mirroring our earlier results (32, 37), loss of accessory chromosomes was 41% and 58% in
479 Δ*ash1* and Δ*kmt5*, respectively. Increased chromosome loss affected some chromosomes more
480 than others. Chromosomes 14 and 16 are easily lost even in wild-type strains, especially under
481 heat stress conditions (32, 35, 37), and they were also lost most commonly, by far, in Δkmt5 and
482 Δash1. Thus, unlike the loss of *kmt6*, which results in an overall more stable genome (32), lack of
483 *ash1* and *kmt5* both resulted in decreased genome stability, which suggests different, separable
484 functions in genome maintenance and control of gene expression in facultative heterochromatin
485 for both Ash1 and Kmt5.

486 Our earlier studies showed that lack of H3K27me3 alone did not result in large-scale upregulation
487 of regions enriched with H3K27me3 (32). One of our goals was to uncover which *Z. tritici* histone
488 modifications, if any, take on the gene silencing function usually mediated by H3K27me3 in other
489 organisms. Here, we showed that H4K20me3, and Ash1-mediated H3K36me3 are important for
490 transcriptional repression of facultative heterochromatin. Some of these effects are phenocopied
491 by replacement of histone H4K20 with a methionine ($H4^{K20M}$), or in a strain with a wild type and
492 H4K20M allele ($H4^{K20/K20M}$). While some *bona fide* genes on core chromosomes and even
493 accessory chromosomes are affected by the lack of Kmt5 or Ash1, most regions enriched with
494 H3K27me3, Ash1-mediated H3K36me3, and H4K20me3 have relatively few previously
495 annotated genes. To understand the transcripts that emanate from these regions we manually
496 curated RNA-seq data for one accessory chromosome. We found that most transcripts arise from
497 sequences that do not appear to be regular genes. How exactly these RNA species act, what
498 their specific functions may be, and whether they interfere or aid propagation of accessory
499 chromosomes in *Z. tritici* goes beyond the scope of the current study. Our results show, however,
500 that studies resulting in a lack of specific histone modifications may necessitate renewed
501 annotation efforts, which should capture transcripts from pseudogenes and apparent *bona fide*
502 genes with few nonsense codons.

503 In conclusion, we showed that H4K20me3, H3K27me3, and Ash1-mediated H3K36me3
504 delineate facultative heterochromatin in *Z. tritici*. H4K20me3, as well as the presence of Eaf3, are
505 essential for Ash1-mediated H3K36me3, uncovering a novel mechanism for establishment and
506 maintenance of facultative heterochromatin and transcriptional silencing.

507 # Methods
508
509 ## Fungal and bacterial growth conditions
510 *Zymoseptoria tritici* cultures were grown on YMS (4 g yeast extract, 4 g malt, 4 g sucrose per
511 liter, with 16 g agar per liter added for solid medium). Glycerol stocks (1:1 YMS and 50 % glycerol)
512 were maintained at -80°C. *Escherichia coli* strain DH10beta (NEB) was grown at 37°C in LB (10 g
513 tryptone, 10 g NaCl, 5 g yeast extract per liter) with appropriate antibiotics (100 µg/mL
514 kanamycin). *Agrobacterium tumefaciens* strain AGL1 was grown in dYT (16 g tryptone, 5 g NaCl,
515 10 g yeast extract per liter) or LB media with appropriate antibiotics (100 µg/mL kanamycin, 100
516 µg/mL carbenicillin, 50 µg/mL rifampicin).
517
518 ## Generation of plasmids for fungal transformation
519 Plasmids were generated by Gibson Assembly (66) using a homemade Gibson reaction mix
520 based on recipes from OpenWetWare (OpenWetWare,
521 https://openwetware.org/wiki/Gibson_Assembly) (5x Isothermal Reaction Mix [600 µL]: 300 µL 1
522 M Tris-HCl [pH 7.5], 30 µL 1 M MgCl2, 6 µL 100 mM dGTP, 6 µL 100 mM dATP, 6 µL 100 mM
523 dTTP, 6 µL 100 mM dCTP, 30 µL 1 M DTT, 0.15 g PEG 8000, 60 µL 50 mM NAD^+, 156 µL H_2O)
524 and modified by using the "enhanced" version (68) (1.33x Gibson-Assembly Master-Mix [for 25
525 reactions]: 100 µL 5x Isothermal Reaction-Mix, 215.32 µL H2O, 0.2 µL T5 Exonuclease [10 U/µL
526 NEB #M0363], 6.25 µL Phusion DNA-Polymerase [2 U/µL ThermoFisher #F530L], 3.125 µL ET
527 SSB [500 µg/ml NEB #M2401S], 50 µL Taq DNA-Ligase [40 U/µL stock NEB #M0208L]). Primers,
528 plasmids, and strains used in this study are listed in Table S3.
529
530 ## Transformation of *Zymoseptoria tritici*
531 Transformation was carried out by *A. tumefaciens* (69). In our updated protocol (detailed
532 protocol is provided as supplemental method), *A. tumefaciens* strain AGL1 (transformed with the
533 respective target plasmid, see Table S3) was grown for ~24 h in liquid culture (LB with 100 µg/mL
534 kanamycin, 100 µg/mL carbenicillin, and 50 µg/mL rifampicin) at 28°C before induction.
535 Induction was performed by centrifuging LB cultures (3000rpm for 5 min), and resuspending cells
536 in 1 mL of induction medium (10 mM K_2HPO_4, 10 mM KH_2PO_4, 2.5 mM NaCl, 2 mM $MgSO_4$, 9
537 µM $FeSO_4$, 40 mM MES buffer, 0.7 mM $CaCl_2$, 0.5 % glycerol, 5 mM glucose, 6.25 mM NH_4NO_3,
538 0.002 % Vogel trace elements, 100 µg/mL kanamycin, 100 µg/mL carbenicillin, 50 µg/mL
539 rifampicin, 200 µM acetosyringone) and inoculating resuspended AGL1 cultures in 5 mL
540 induction medium (OD_{590} = 0.15) for overnight growth at 28°C. Induced cultures were adjusted
541 to OD_{590} = 0.4 the following day and mixed with *Z. tritici* cells (OD_{590} = 1) at a 1:1 ratio. To grow
542 recipient *Z. tritici* cells for this step, spores were streaked out on YMS plates from glycerol stocks
543 3-4 days before transformation, resuspended in water, and the concentration adjusted to an
544 OD_{590} = 1 in induction medium, before mixing with induced AGL1 cells. Aliquots of 250 µL of
545 the *A. tumefaciens* AGL1 and *Z. tritici* mixture were plated on Hybond N+ membranes on plates
546 with induction medium and incubated at room temperature for 48-72 h. Membranes were
547 transferred to YMS plates containing the appropriate antibiotics for selection (250 µg/mL

548 cefotaxime, 150 µg/mL timentin, 100 µg/mL G418, 100 µg/mL hygromycin) and incubated for
549 another ~10 days at 18°C until resistant colonies appeared.
550
551 **Chromatin immunoprecipitation and sequencing (ChIP-seq)**
552 ChIP experiments were carried out as described previously (70) with some modifications; a
553 detailed protocol is provided as supplemental method. Briefly, fungal spores were grown on
554 YMS plates for three to four days, harvested, and resuspended in 5 mL of 1x PBS (137 mM NaCl,
555 2.7 mM KCl, 10 mM Na_2HPO_4, 1.8 mM KH_2PO_4). Cells were crosslinked using 0.5% formaldehyde
556 for 15 min at room temperature and quenched by adding 150 µL of 2.5 M glycine. Crosslinked
557 cells were centrifuged at 3,000 rpm for 5 min at 4°C and washed once with cold 1x PBS. We
558 found that grinding cell pellets to a fine powder in liquid nitrogen and storage at -80°C resulted
559 in no noticeable decrease in ChIP efficiency (storage for at least six months was acceptable). For
560 ChIP, frozen, ground cells were resuspended in ice-cold ChIP lysis buffer (50 mM HEPES-NaOH
561 [pH 7.5], 90 mM NaCl, 1 mM Na-EDTA [pH 8.0], 1% Triton X-100, 0.1% DOC, and proteinase
562 inhibitors [1 mM PMSF, 1 µg/mL Leupeptin, 1 µg/mL E-64 and 0.1 µg/mL Pepstatin]) in a ratio of
563 5 µL ChIP lysis buffer to 1 mg of ground cells. To 1 mL of lysate, 2 µL 1 M $CaCl_2$ and 5 µL
564 micrococcal nuclease (NEB, #M0247S) were added and chromatin was fragmented into
565 predominantly mono-nucleosomes by incubation at 37°C for 15 min. The reaction was stopped
566 by adding 20 µL of 0.5 M Na-EGTA, pH 8. Digested chromatin was centrifuged at 6,000 rpm for
567 5 min and 250-300 µL of the supernatant was used per ChIP reaction. Chromatin was pre-cleared
568 by incubating with protein A Dynabeads (Invitrogen) at 4°C for 1 h followed by overnight
569 incubation with 3 µL of the following antibodies: H3K4me2 (Millipore 07-030), H3K9me3 (Active
570 Motif 39161), H3K27me3 (Active Motif 39155), H3K27me2 (Active Motif 39245), H3K36me2
571 (Active Motif 39255; abcam 9049), H3K36me3 (Active Motif 61101; abcam 9050), H4K20me1
572 (abcam 9051), H4K20me3 (Active Motif 91107). After overnight incubation, 25 µL protein A
573 Dynabeads were added and samples were incubated for 1-2 h at 4°C. Beads were washed twice
574 with ChIP lysis buffer, once with ChIP lysis buffer + 0.5 M NaCl (50 mM HEPES-NaOH [pH 7.5],
575 500 mM NaCl, 1 mM Na-EDTA [pH 8.0], 1% Triton X-100, 0.1% DOC), once with LiCl wash buffer
576 (10 mM Tris-HCl [pH 8.0], 250 mM LiCl, 0.5 % IGEPAL CA-630, 0.5 % DOC, 1 mM Na-EDTA [pH
577 8]) and once with 1x TE buffer. Chromatin was eluted in 125 µL TES (50 mM Tris-HCl [pH 8.0], 10
578 mM Na-EDTA [pH 8], 1% SDS) and de-crosslinked overnight at 65°C. Samples were treated with
579 RNAse A (2 h at 50°C) and proteinase K (2 h at 65°C) and DNA was extracted with the ChIP DNA
580 Clean & Concentrator kit (Zymo Research). Libraries for sequencing were prepared with a
581 modified version of the Next Ultra II DNA Library Prep Kit for Illumina (NEB, #E7645S).
582 Sequencing was performed on an Illumina HiSeq 3000, obtaining 2 x 150-nt read pairs by
583 Admera Health (South Plainfield, NJ, USA).
584
585 **RNA isolation and sequencing (RNA-seq)**
586 Fungal cells were grown and harvested as described for the ChIP experiments. Cells were ground
587 in liquid nitrogen and ~100 mg of ground cells were used for total RNA extraction by a TRIZOL
588 (Invitrogen) method. Extraction was carried out according to the manufacturer's instructions and
589 total RNA was treated with DNAse I. Stranded mRNA libraries were prepared by a modified
590 version of a previously published protocol (71); the detailed protocol is provided as supplemental

591 method. Stranded mRNA libraries were sent to Admera Health (South Plainfield, NJ, USA) for
592 sequencing on an Illumina HiSeq 3000, obtaining 2 x 150-nt read pairs.
593
594 Quantification of chromosome loss
595 Each strain (wild type, Δ*kmt5*, Δ*ash1*) was grown in five replicate populations on YMS plates, and
596 every three to four days a fraction of the population was transferred to a new plate. After eight
597 transfers (four weeks), populations were diluted and spread on YMS plates to obtain single
598 colonies, representing individual cells of the respective population. A total of 48
599 colonies/replicate (i.e., 240 per strain) were screened by PCR for the presence of all accessory
600 chromosomes as previously described (37).
601
602 Western blots
603 Fungal cells were grown on YMS plates for three to four days, harvested and washed in 1x PBS.
604 Cells were resuspended in three volumes of high-salt extraction buffer (25 mM HEPES-NaOH
605 [pH 7.9], 700 mM NaCl, 0.1 mM Na-EDTA [pH 8.0], 0.2% NP-40, 20% glycerol, 1.5 mM $MgCl_2$,
606 1 mM PMSF, 1 mM DTT, 1 µg/mL Leupeptin, 0.1 µg/mL Pepstatin) and incubated on ice for 10
607 min. Samples were sonicated (Branson Sonifier-450) for three sets of 10 pulses (output = 2, duty
608 cycle = 80), keeping the sample on ice between sets. Insoluble material was removed by
609 centrifugation at 14,000 rpm and 4°C for 10 min. Protein concentrations were quantified with a
610 Qubit fluorimeter (Invitrogen). Total protein (75 µg per lane) was loaded onto pre-cast 4-20%
611 gradient Mini-PROTEAN TGX Stain-Free SDS PAGE gels (BioRad). Proteins were transferred onto
612 nitrocellulose membrane (0.2 µm pore size; BioTrace) by wet transfer (1 h, 110V). The following
613 primary antibodies were used: αH3 (Active motif 39763, mAb, 1:5000), αH4K20me1 (abcam
614 9051, pAb, 1:1000), αH4K20me3 (Active motif 39180, pAb, 1:2000). The following secondary
615 antibodies were used: IRDye 680RD Goat anti-Mouse IgG (LI-COR 926-68070, 1:5000), IRDye
616 800CW Goat anti-Rabbit IgG (LI-COR 926-32211, 1:5000). Fluorescent signals were detected
617 using a LI-COR Odyssey CLx imager.
618
619 Hi-C analyses
620 WT and Δ*kmt6* cells were grown as described for ChIP experiments. Hi-C experiments were
621 carried out using the Phase Genomics Proximo Hi-C Kit (Microbe) following the instructions for
622 fungal samples; the Proximo Hi-C Kit (Fungal) had not been officially released when we carried
623 out our experiments. *Dpn*II was used as restriction enzyme. Libraries were generated and size-
624 selected according to the Phase Genomics kit instructions. Libraries were sent for sequencing to
625 Phase Genomics, obtaining ~100 million 2 x 100-nt reads per sample.
626
627 Phenotypic responses to genotoxic stress
628 Fungal cells were grown on YMS plates for three to four days and diluted to OD_{590} = 1 in water
629 (~10^7 cells/mL and tenfold dilution series to 100 cells/mL); 3 µL of the spore dilutions were
630 pipetted onto plates. Pictures were taken after 7 and 12 days of growth (18°C, 28°C, and RT
631 [~23°C]). To test for responses to different genotoxic stressors *in vitro*, YMS plates containing
632 hydroxyurea (HU; 100 µM, 1 mM, 10 mM), camptothecin (1 mM, 10 mM, 100 mM), and methyl

633 methanesulfonate (MMS; 0.005% and 0.0075%) and three plates containing only YMS were
634 prepared.
635
636 Data analyses
637 Detailed descriptions of software and commands for analyses of ChIP-seq, RNA-seq and Hi-C
638 data can be found as supplementary methods. A list of all sequencing datasets can be found in
639 Table S4.
640 *ChIP-seq*
641 ChIP-seq data were quality-filtered and adapters removed with trimmomatic v.0.39 (72).
642 Mapping was performed with bowtie2 v.2.4.4 (73), and sorting and indexing with samtools v.1.9
643 (74). Normalized coverage bigwig files and heatmaps were created with deeptools v.3.5.1 (75).
644 Wiggletools v.1.2 and the UCSC Genome Browser tools were used to calculate means for
645 replicates and converting wig to bigwig files. Peaks were called with homer v4.11.1 (76) and
646 bedtools v2.30.0 were used to make windows and intersect peaks with genomic features.
647 *RNA-seq*
648 RNA-seq data were quality filtered and adapters removed with trimmomatic v.0.39 (72). Mapping
649 of all paired reads was performed with hisat2 2.1.0 (77), and sorting and indexing with samtools
650 v.1.9 (74). HTSeq v.0.11.2 (78) was used to count reads on features. The *Z. tritici* IPO323 gene
651 annotation was obtained from FungiDB (release 53) (79), based on previous annotations (80).
652 Differential expression analyses was conducted with DEseq2 v.1.32.0 (81), see supplemental R
653 script. New transcripts were annotated by combining all mapped RNA-seq data with stringtie v.
654 v2.2.1 (49). Manual annotation was done by combining all RNA-seq data and extracting transcript
655 sequences that were > 200 bp in length and supported by at least 10 reads with IGV (82) and
656 Geneious (83). Transcripts were characterized by blastn with the *Z. tritici* genome as a reference
657 to find homologous sequences on core and accessory chromosomes and blastx to find homologs
658 in other species and to infer functional annotations.
659 *Hi-C*
660 HiCUP v0.8.3 (84) was used to trim and map the data, see supplemental config file. Homer
661 v4.11.1 (76) was used to extract valid Hi-C interactions and generating normalized interaction
662 matrices. Treeview3 (85) was used to visualize Hi-C data.
663
664 Data availability
665 Sequencing raw reads (FASTQ files) of all ChIP-seq, RNA-seq and Hi-C data are available online
666 at Sequence Read Archive (SRA) under BioProject ID PRJNA902413.
667 Normalized bigwig files for all ChIP-seq datasets, reference genome and annotations have been
668 deposited at zenodo under doi: 10.5281/zenodo.7460287.

669 Acknowledgements
670 We thank Eva Stukenbrock for supplying critical materials and strains, and for supporting this
671 work while MM was still at CAU Kiel. We thank colleagues in the Freitag lab and Zachary Lewis
672 (University of Georgia) for conversations and comments on the manuscript. MM was supported
673 by a grant from the DFG (MO 3755/1-1). JBR was supported by a grant from USDA-AFRI (2019-
674 67012-29722). Chromatin research in the Freitag lab is supported by grants from the NSF
675 (MCB1818006), NIH (R01GM132644), and the BSF (#2019034) to MF.
676
677 Competing interests
678 The authors declare that no competing interests exist.
679

680 # References

681
682 1. Jenuwein T, Allis CD (2001) Translating the histone code. *Science* 293(5532):1074–80.
683 2. Liu C, et al. (2016) Genome-wide analysis of chromatin packing in Arabidopsis thaliana at
684 single-gene resolution. *Genome Res* 26(8):1057–1068.
685 3. Cheutin T, Cavalli G (2012) Progressive Polycomb Assembly on H3K27me3
686 Compartments Generates Polycomb Bodies with Developmentally Regulated Motion.
687 *PLOS Genet* 8(1):e1002465.
688 4. Pauler FM, et al. (2009) H3K27me3 forms BLOCs over silent genes and intergenic
689 regions and specifies a histone banding pattern on a mouse autosomal chromosome.
690 *Genome Res* 19(2):221–233.
691 5. Connolly LR, Smith KM, Freitag M (2013) The Fusarium graminearum histone H3 K27
692 methyltransferase KMT6 regulates development and expression of secondary metabolite
693 gene clusters. *PLoS Genet* 9(10):e1003916.
694 6. Schotanus K, et al. (2015) Histone modifications rather than the novel regional
695 centromeres of Zymoseptoria tritici distinguish core and accessory chromosomes.
696 *Epigenetics Chromatin* 8:41.
697 7. Żylicz JJ, Heard E (2020) Molecular Mechanisms of Facultative Heterochromatin
698 Formation: An X-Chromosome Perspective. *Annu Rev Biochem* 89(1):255–282.
699 8. Trojer P, Reinberg D (2007) Facultative Heterochromatin: Is There a Distinctive Molecular
700 Signature? *Mol Cell* 28(1):1–13.
701 9. Blackledge NP, et al. (2014) Variant PRC1 Complex-Dependent H2A Ubiquitylation
702 Drives PRC2 Recruitment and Polycomb Domain Formation. *Cell* 157(6):1445–1459.
703 10. Ridenour JB, Möller M, Freitag M (2020) Polycomb Repression without Bristles:
704 Facultative Heterochromatin and Genome Stability in Fungi. *Genes (Basel)* 11(6).
705 doi:10.3390/genes11060638.
706 11. Corvalan AZ, Coller HA (2020) Methylation of histone 4's lysine 20: a critical analysis of
707 the state of the field. *Physiol Genomics* 53(1):22–32.
708 12. Fang J, et al. (2002) Purification and Functional Characterization of SET8, a Nucleosomal
709 Histone H4-Lysine 20-Specific Methyltransferase. *Curr Biol* 12(13):1086–1099.
710 13. Nishioka K, et al. (2002) PR-Set7 Is a Nucleosome-Specific Methyltransferase that

711 Modifies Lysine 20 of Histone H4 and Is Associated with Silent Chromatin. *Mol Cell*
712 9(6):1201–1213.
713 14. Schotta G, et al. (2008) A chromatin-wide transition to H4K20 monomethylation impairs
714 genome integrity and programmed DNA rearrangements in the mouse. *Genes Dev*
715 22(15):2048–2061.
716 15. Yang H, et al. (2008) Preferential dimethylation of histone H4 lysine 20 by Suv4-20. *J Biol*
717 *Chem* 283(18):12085–12092.
718 16. Sanders SL, et al. (2004) Methylation of Histone H4 Lysine 20 Controls Recruitment of
719 Crb2 to Sites of DNA Damage. *Cell* 119(5):603–614.
720 17. Bachleitner S, Sulyok M, Sørensen JL, Strauss J, Studt L (2021) The H4K20
721 methyltransferase Kmt5 is involved in secondary metabolism and stress response in
722 phytopathogenic Fusarium species. *Fungal Genet Biol* 155:103602.
723 18. Pham KTM, et al. (2015) MoSET1 (Histone H3K4 Methyltransferase in Magnaporthe
724 oryzae) Regulates Global Gene Expression during Infection-Related Morphogenesis.
725 *PLOS Genet* 11(7):e1005385.
726 19. Beck DB, et al. (2012) The role of PR-Set7 in replication licensing depends on Suv4-20h.
727 *Genes Dev* 26(23):2580–2589.
728 20. Jørgensen S, Schotta G, Sørensen CS (2013) Histone H4 Lysine 20 methylation: Key
729 player in epigenetic regulation of genomic integrity. *Nucleic Acids Res* 41(5):2797–2806.
730 21. Brustel J, et al. (2017) Histone H4K20 tri-methylation at late-firing origins ensures timely
731 heterochromatin replication. *EMBO J* 36(18):2726–2741.
732 22. Evertts AG, et al. (2013) H4K20 methylation regulates quiescence and chromatin
733 compaction. *Mol Biol Cell* 24(19):3025–3037.
734 23. Chai X, Nagarajan S, Kim K, Lee K, Choi JK (2013) Regulation of the boundaries of
735 accessible chromatin. *PLoS Genet* 9(9):e1003778.
736 24. Shoaib M, et al. (2021) Histone H4 lysine 20 mono-methylation directly facilitates
737 chromatin openness and promotes transcription of housekeeping genes. *Nat Commun*
738 12(1):4800.
739 25. Morris SA, et al. (2005) Histone H3 K36 methylation is associated with transcription
740 elongation in Schizosaccharomyces pombe. *Eukaryot Cell* 4(8):1446–1454.
741 26. Dorighi KM, Tamkun JW (2013) The trithorax group proteins Kismet and ASH1 promote
742 H3K36 dimethylation to counteract Polycomb group repression in Drosophila.
743 *Development* 140(20):4182–4192.
744 27. Li Y, et al. (2009) The Target of the NSD Family of Histone Lysine Methyltransferases
745 Depends on the Nature of the Substrate. *J Biol Chem* 284(49):34283–34295.
746 28. Yuan W, et al. (2011) H3K36 Methylation Antagonizes PRC2-mediated H3K27
747 Methylation. *J Biol Chem* 286(10):7983–7989.
748 29. Dorafshan E, et al. (2019) Ash1 counteracts Polycomb repression independent of histone
749 H3 lysine 36 methylation. *EMBO Rep* 20(4). doi:10.15252/embr.201846762.
750 30. Bicocca VT, Ormsby T, Adhvaryu KK, Honda S, Selker EU (2018) ASH1-catalyzed H3K36
751 methylation drives gene repression and marks H3K27me2/3-competent chromatin. *Elife*
752 7:1–19.
753 31. Janevska S, et al. (2018) Elucidation of the Two H3K36me3 Histone Methyltransferases

754 Set2 and Ash1 in Fusarium fujikuroi Unravels Their Different Chromosomal Targets and a
755 Major Impact of Ash1 on Genome Stability. *Genetics* 208(1):153 LP – 171.
756 32. Möller M, et al. (2019) Destabilization of chromosome structure by histone H3 lysine 27
757 methylation. *PLOS Genet* 15(4):e1008093.
758 33. Möller M, et al. (2021) Recent loss of the Dim2 DNA methyltransferase decreases
759 mutation rate in repeats and changes evolutionary trajectory in a fungal pathogen. *PLOS*
760 *Genet* 17(3):e1009448.
761 34. Goodwin SB, et al. (2011) Finished Genome of the Fungal Wheat Pathogen
762 Mycosphaerella graminicola Reveals Dispensome Structure, Chromosome Plasticity, and
763 Stealth Pathogenesis. *PLoS Genet* 7(6):e1002070.
764 35. Habig M, Lorrain C, Feurtey A, Komluski J, Stukenbrock EH (2021) Epigenetic
765 modifications affect the rate of spontaneous mutations in a pathogenic fungus. *Nat*
766 *Commun* 12(1):5869.
767 36. Dorafshan E, Kahn TG, Glotov A, Savitsky M, Schwartz YB (2019) Genetic Dissection
768 Reveals the Role of Ash1 Domains in Counteracting Polycomb Repression. *G3*
769 *Genes|Genomes|Genetics* 9(11):3801–3812.
770 37. Möller M, Habig M, Freitag M, Stukenbrock EH (2018) Extraordinary Genome Instability
771 and Widespread Chromosome Rearrangements During Vegetative Growth. *Genetics*
772 210 no. 2:517–529.
773 38. Winter DJ, et al. (2018) Repeat elements organise 3D genome structure and mediate
774 transcription in the filamentous fungus Epichloë festucae. *PLOS Genet* 14(10):e1007467.
775 39. Klocko AD, et al. (2016) Normal chromosome conformation depends on subtelomeric
776 facultative heterochromatin in *Neurospora crassa*. *Proc Natl Acad Sci* 113(52):15048–
777 15053.
778 40. Galazka JM, et al. (2016) *Neurospora* chromosomes are organized by blocs of importin
779 alpha- dependent heterochromatin that are largely independent of H3K9me3. *Genome*
780 *Res* (541):1069–1080.
781 41. Varoquaux N, et al. (2015) Accurate identification of centromere locations in yeast
782 genomes using Hi-C. *Nucleic Acids Res* 43(11):5331–5339.
783 42. Wang Y, et al. (2009) Regulation of Set9-Mediated H4K20 Methylation by a PWWP
784 Domain Protein. *Mol Cell* 33(4):428–437.
785 43. Wiles ET, Mumford CC, McNaught KJ, Tanizawa H, Selker EU (2022) The ACF chromatin
786 remodeling complex is essential for Polycomb repression. *Elife* 11:e77595.
787 44. Carrozza MJ, et al. (2005) Histone H3 methylation by Set2 directs deacetylation of
788 coding regions by Rpd3S to suppress spurious intragenic transcription. *Cell* 123(4):581–
789 592.
790 45. Eisen A, et al. (2001) The yeast NuA4 and Drosophila MSL complexes contain
791 homologous subunits important for transcription regulation. *J Biol Chem* 276(5):3484–
792 3491.
793 46. Xu C, Cui G, Botuyan MV, Mer G (2008) Structural basis for the recognition of
794 methylated histone H3K36 by the Eaf3 subunit of histone deacetylase complex Rpd3S.
795 *Structure* 16(11):1740–1750.
796 47. Huang C, et al. (2017) Mrg15 stimulates Ash1 H3K36 methyltransferase activity and

797 facilitates Ash1 Trithorax group protein function in Drosophila. *Nat Commun* 8(1):1649.
798 48. Cao X, et al. (2020) Histone H4K20 Demethylation by Two hHR23 Proteins. *Cell Rep*
799 30(12):4152-4164.e6.
800 49. Pertea M, Kim D, Pertea GM, Leek JT, Salzberg SL (2016) Transcript-level expression
801 analysis of RNA-seq experiments with HISAT, StringTie and Ballgown. *Nat Protoc*
802 11(9):1650–1667.
803 50. Grandaubert J, Bhattacharyya A, Stukenbrock EH (2015) RNA-seq based gene
804 annotation and comparative genomics of four fungal grass pathogens in the genus
805 Zymoseptoria identify novel orphan genes and species-specific invasions of transposable
806 elements. *G3* 5:1323–1333.
807 51. Yang H, Kwon CS, Choi Y, Lee D (2016) Both H4K20 mono-methylation and H3K56
808 acetylation mark transcription-dependent histone turnover in fission yeast. *Biochem*
809 *Biophys Res Commun* 476(4):515–521.
810 52. Congdon LM, Houston SI, Veerappan CS, Spektor TM, Rice JC (2010) PR-Set7-mediated
811 monomethylation of histone H4 lysine 20 at specific genomic regions induces
812 transcriptional repression. *J Cell Biochem* 110(3):609–619.
813 53. Tjalsma SJD, et al. (2021) H4K20me1 and H3K27me3 are concurrently loaded onto the
814 inactive X chromosome but dispensable for inducing gene silencing. *EMBO Rep*
815 22(3):e51989.
816 54. Nelson DM, et al. (2016) Mapping H4K20me3 onto the chromatin landscape of
817 senescent cells indicates a function in control of cell senescence and tumor suppression
818 through preservation of genetic and epigenetic stability. *Genome Biol* 17(1):158.
819 55. Fraga MF, et al. (2005) Loss of acetylation at Lys16 and trimethylation at Lys20 of histone
820 H4 is a common hallmark of human cancer. *Nat Genet* 37(4):391–400.
821 56. Benetti R, et al. (2007) Suv4-20h deficiency results in telomere elongation and
822 derepression of telomere recombination. *J Cell Biol* 178(6):925–936.
823 57. Schotta G, et al. (2004) A silencing pathway to induce H3-K9 and H4-K20 trimethylation
824 at constitutive heterochromatin. *Genes Dev* 18:1251–1262.
825 58. Xu J, Kidder BL (2018) H4K20me3 co-localizes with activating histone modifications at
826 transcriptionally dynamic regions in embryonic stem cells. *BMC Genomics* 19(1):514.
827 59. van Kruijsbergen I, et al. (2017) Heterochromatic histone modifications at transposons in
828 Xenopus tropicalis embryos. *Dev Biol* 426(2):460–471.
829 60. Grau-Bové X, et al. (2022) A phylogenetic and proteomic reconstruction of eukaryotic
830 chromatin evolution. *Nat Ecol Evol* 6(7):1007–1023.
831 61. Justin N, et al. (2016) Structural basis of oncogenic histone H3K27M inhibition of human
832 polycomb repressive complex 2. *Nat Commun* 7(1):11316.
833 62. Jiao L, Liu X (2015) Structural basis of histone H3K27 trimethylation by an active
834 polycomb repressive complex 2. *Science (80-)* 350(6258):aac4383.
835 63. Hou P, et al. (2019) Structural Insights into Stimulation of Ash1L's H3K36
836 Methyltransferase Activity through Mrg15 Binding. *Structure* 27(5):837-845.e3.
837 64. Nakamura K, et al. (2019) H4K20me0 recognition by BRCA1–BARD1 directs homologous
838 recombination to sister chromatids. *Nat Cell Biol* 21(3):311–318.
839 65. Shoaib M, et al. (2018) Histone H4K20 methylation mediated chromatin compaction

840 threshold ensures genome integrity by limiting DNA replication licensing. *Nat Commun*
841 9(1). doi:10.1038/s41467-018-06066-8.
842 66. Gibson DG, et al. (2009) Enzymatic assembly of DNA molecules up to several hundred
843 kilobases. *Nat Methods* 6(5):343–345.
844 67. OpenWetWare Gibson Assembly. Available at:
845 https://openwetware.org/wiki/Gibson_Assembly [Accessed October 14, 2022].
846 68. Rabe BA, Cepko C (2020) A Simple Enhancement for Gibson Isothermal Assembly.
847 *bioRxiv*:2020.06.14.150979.
848 69. Poppe S, Dorsheimer L, Happel P, Stukenbrock EH (2015) Rapidly Evolving Genes Are
849 Key Players in Host Specialization and Virulence of the Fungal Wheat Pathogen
850 Zymoseptoria tritici (Mycosphaerella graminicola). *PLoS Pathog* 11(7):1–21.
851 70. Soyer JL, et al. (2015) Chromatin analyses of Zymoseptoria tritici: Methods for chromatin
852 immunoprecipitation followed by high-throughput sequencing (ChIP-seq). *Fungal Genet*
853 *Biol* 79:63–70.
854 71. Zhong S, et al. (2011) High-throughput illumina strand-specific RNA sequencing library
855 preparation. *Cold Spring Harb Protoc* 2011(8):940–949.
856 72. Bolger AM, Lohse M, Usadel B (2014) Trimmomatic: A flexible trimmer for Illumina
857 sequence data. *Bioinformatics* 30(15):2114–2120.
858 73. Langmead B, Salzberg SL (2012) Fast gapped-read alignment with Bowtie 2. *Nat*
859 *Methods* 9(4):357–359.
860 74. Li H (2011) A statistical framework for SNP calling, mutation discovery, association
861 mapping and population genetical parameter estimation from sequencing data.
862 *Bioinformatics* 27(21):2987–2993.
863 75. Ramírez F, et al. (2016) deepTools2: a next generation web server for deep-sequencing
864 data analysis. *Nucleic Acids Res* 44(W1):W160–W165.
865 76. Heinz S, et al. (2010) Simple Combinations of Lineage-Determining Transcription Factors
866 Prime cis-Regulatory Elements Required for Macrophage and B Cell Identities. *Mol Cell*
867 38(4):576–589.
868 77. Kim D, Paggi JM, Park C, Bennett C, Salzberg SL (2019) Graph-based genome
869 alignment and genotyping with HISAT2 and HISAT-genotype. *Nat Biotechnol* 37(8):907–
870 915.
871 78. Anders S, Pyl PT, Huber W (2015) HTSeq-A Python framework to work with high-
872 throughput sequencing data. *Bioinformatics* 31(2):166–169.
873 79. Basenko EY, et al. (2018) FungiDB: An Integrated Bioinformatic Resource for Fungi and
874 Oomycetes. *J Fungi* 4(1). doi:10.3390/jof4010039.
875 80. Grandaubert J, Bhattacharyya A, Stukenbrock EH (2015) RNA-seq Based Gene
876 Annotation and Comparative Genomics of Four Fungal Grass Pathogens in the Genus
877 Zymoseptoria Identify Novel Orphan Genes and Species-Specific Invasions of
878 Transposable Elements. *G3 (Bethesda)* 5(July):g3.115.017731-.
879 81. Love MI, Huber W, Anders S (2014) Moderated estimation of fold change and dispersion
880 for RNA-seq data with DESeq2. *Genome Biol* 15(12):1–21.
881 82. Thorvaldsdóttir H, Robinson JT, Mesirov JP (2013) Integrative Genomics Viewer (IGV):
882 High-performance genomics data visualization and exploration. *Brief Bioinform*

883 14(2):178–192.
884 83. Kearse M, et al. (2012) Geneious Basic: An integrated and extendable desktop software
885 platform for the organization and analysis of sequence data. *Bioinformatics* 28(12):1647–
886 1649.
887 84. Wingett SW, et al. (2015) HiCUP: pipeline for mapping and processing Hi-C data [version
888 1; peer review: 2 approved, 1 approved with reservations]. *F1000Research* 4(1310).
889 doi:10.12688/f1000research.7334.1.
890 85. Keil C, et al. (2018) Treeview 3.0 (beta 1) - Visualization and analysis of large data
891 matrices. *zenodo*. doi:doi:10.5281/zenodo.1303402.
892

893 # Tables

894 **Table 1:** Chromosome loss in wild-type, Δ*kmt5* and Δ*ash1* strains. Chromosome loss is tabulated
895 by individual chromosome and as the sum of all losses (loss), compared to strains without
896 chromosome loss (no loss). Overall chromosome loss frequency (% loss) was calculated as
897 (loss/total tested) *100. Some strains lost multiple chromosomes.

	WT	Δ*kmt5*	Δ*ash1*
chromosome 14	2	107	17
chromosome 15	3	4	1
chromosome 16	2	60	89
chromosome 17	0	4	0
chromosome 19	0	0	0
chromosome 20	1	0	2
chromosome 21	0	0	0
total tested	240	240	240
loss	8	140	99
no loss	232	100	141
loss frequency (%)	3	58	41

898
899
900
901 **Table 2:** Manual annotation of transcripts expressed on chromosome 17 based on RNA-seq data
902 of wild type and mutants.

	number of transcripts
identified	186
protein coding	13
homologs on accessory chromosomes	89
homologs on core chromosomes	62
homologs in other (fungal) species	41
functional annotation	31

903

904 # Figures

905

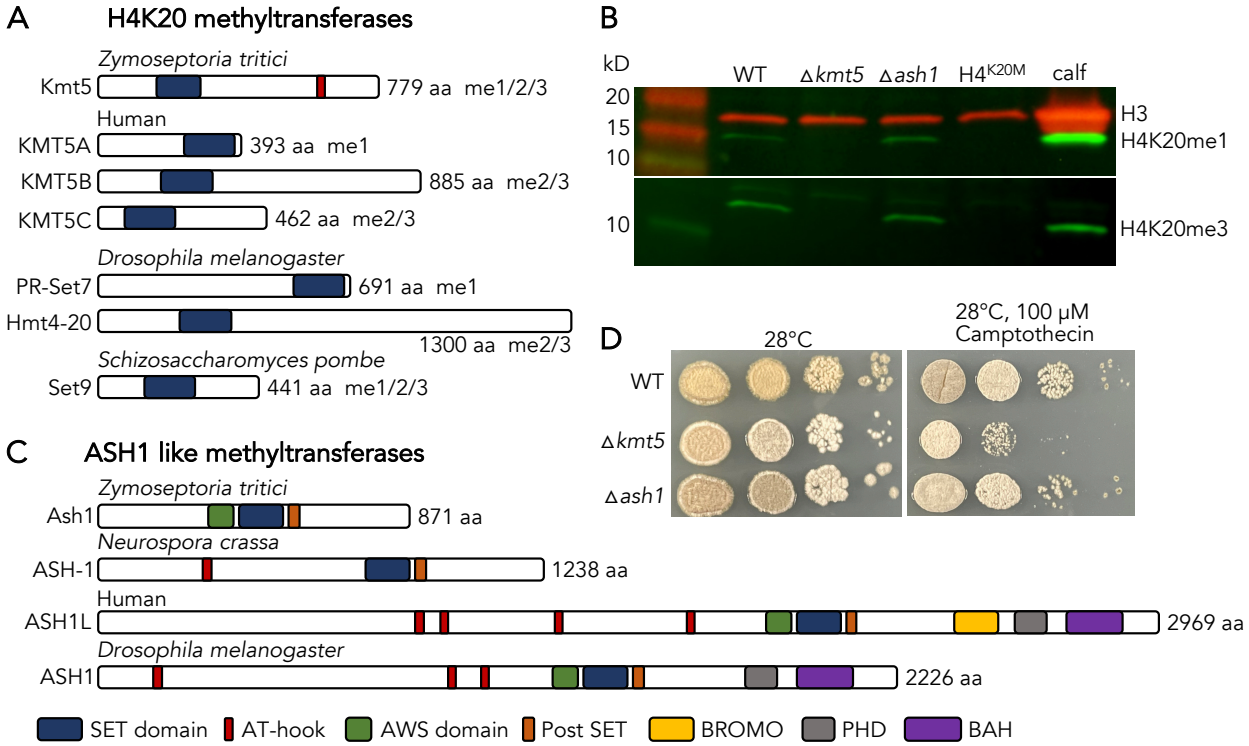

906
907 **Figure 1. Domain structure and characterization of defects related to two histone**
908 **methyltransferases involved in generation of facultative heterochromatin. A)** Comparison of
909 H4K20 methyltransferases related to Kmt5 (accession numbers in Figure S1B). The blue box
910 denotes the SET domain. **B)** Deletion of *kmt5* and substitution of H4 lysine 20 with methionine
911 (H4K20M) causes complete loss of H4K20 methylation but *ash1* deletion has no effect on H4K20
912 methylation. Calf thymus histones were used as controls. **C)** Comparison of H3K36 Ash1
913 methyltransferases. **D)** *kmt5* but not *ash1* mutants are mildly affected by the DNA replication
914 inhibitor camptothecin at high temperature.

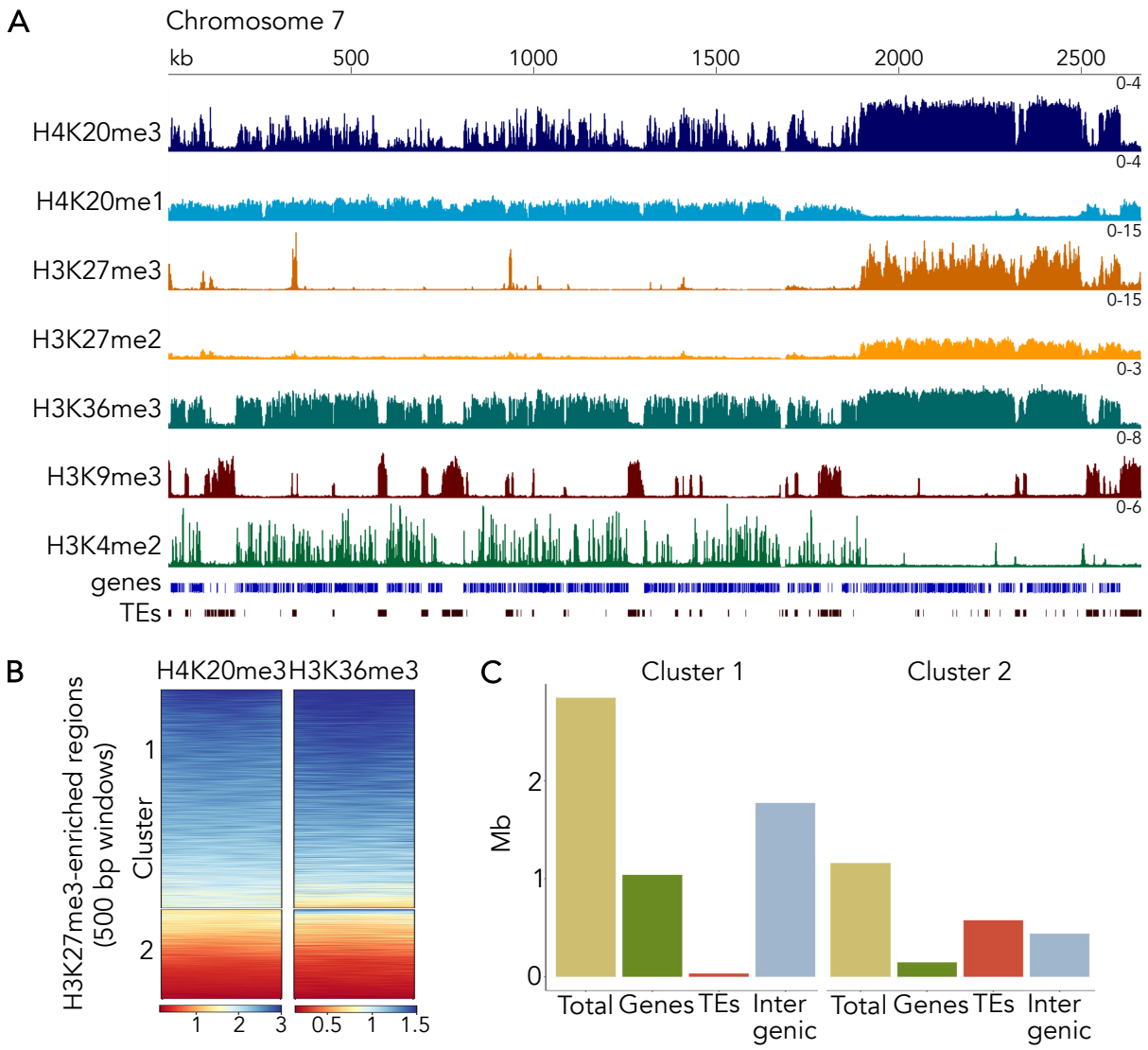

Figure 2: Characterization of different histone modification patterns and their genomic context. **A)** Distribution of selected histone modifications on chromosome 7 in the wild-type *Zymoseptoria tritici* strain. In facultative heterochromatin regions, H4K20me3, H3K27me2/3 and H3K36me3 overlap. **B)** Enrichment of H3K36me3 and H4K20me3 within H3K27me3 regions. There are two distinct clusters, regions where H3K36me3 and H4K20me3 co-occur (cluster 1) and regions where both marks are absent or only one of them is present (cluster 2). **C)** Genomic context of cluster 1 and 2; Mb, million base pairs.

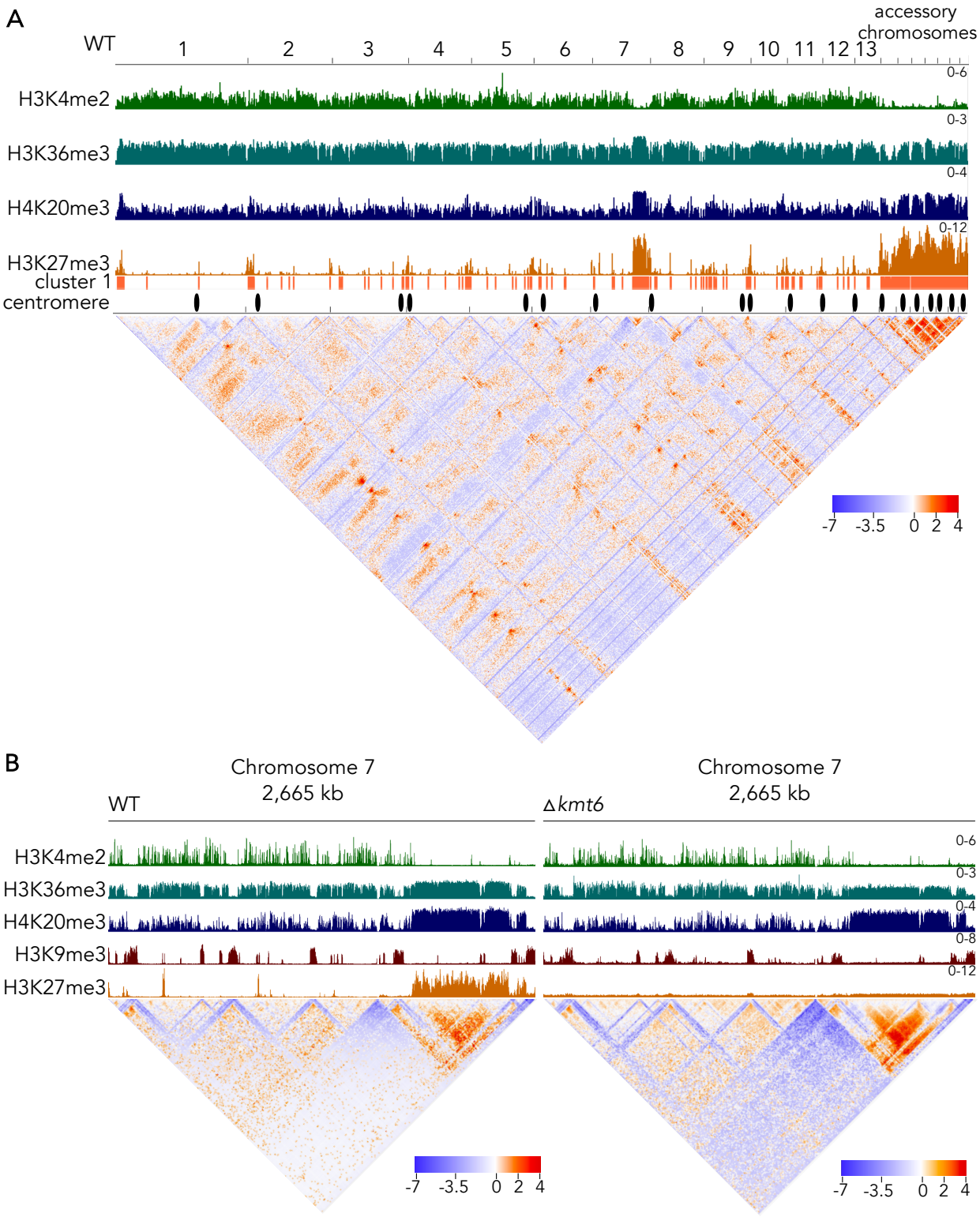
A
WT
1
2
3
4
5
6
7
8
9
10
11
12
13
accessory chromosomes
H3K4me2
0-6
H3K36me3
0-3
H4K20me3
0-4
H3K27me3
0-12
cluster 1
centromere
-7
-3.5
0
2
4
B
Chromosome 7
2,665 kb
WT
Chromosome 7
2,665 kb
Δkmt6
H3K4me2
H3K36me3
H4K20me3
H3K9me3
H3K27me3
0-6
0-3
0-4
0-8
0-12
-7
-3.5
0
2
4
-7
-3.5
0
2
4

923
924

925 **Figure 3: Genome-wide and chromosome-specific Hi-C interaction map in wild-type and Δkmt6**
926 **mutant. A)** Interacting genomic regions in the wild-type genome. Shown are log_2 ratios of
927 observed interactions relative to expected interactions; fewer interactions than expected are
928 colored in blue and more interactions than expected are colored in red. Most centromeres (6)
929 and regions of facultative heterochromatin (cluster 1) show strong interactions. **B)** Side-by-side
930 comparison of interactions on chromosome 7 in wild-type and the Δ*kmt6* mutant. The right arm
931 of chromosome 7 shows strong regional interactions but very few interactions with the left arm
932 of the chromosome. The interacting region correlates with H3K27me3 enrichment in WT, but
933 interactions do not change in absence of H3K27me3.

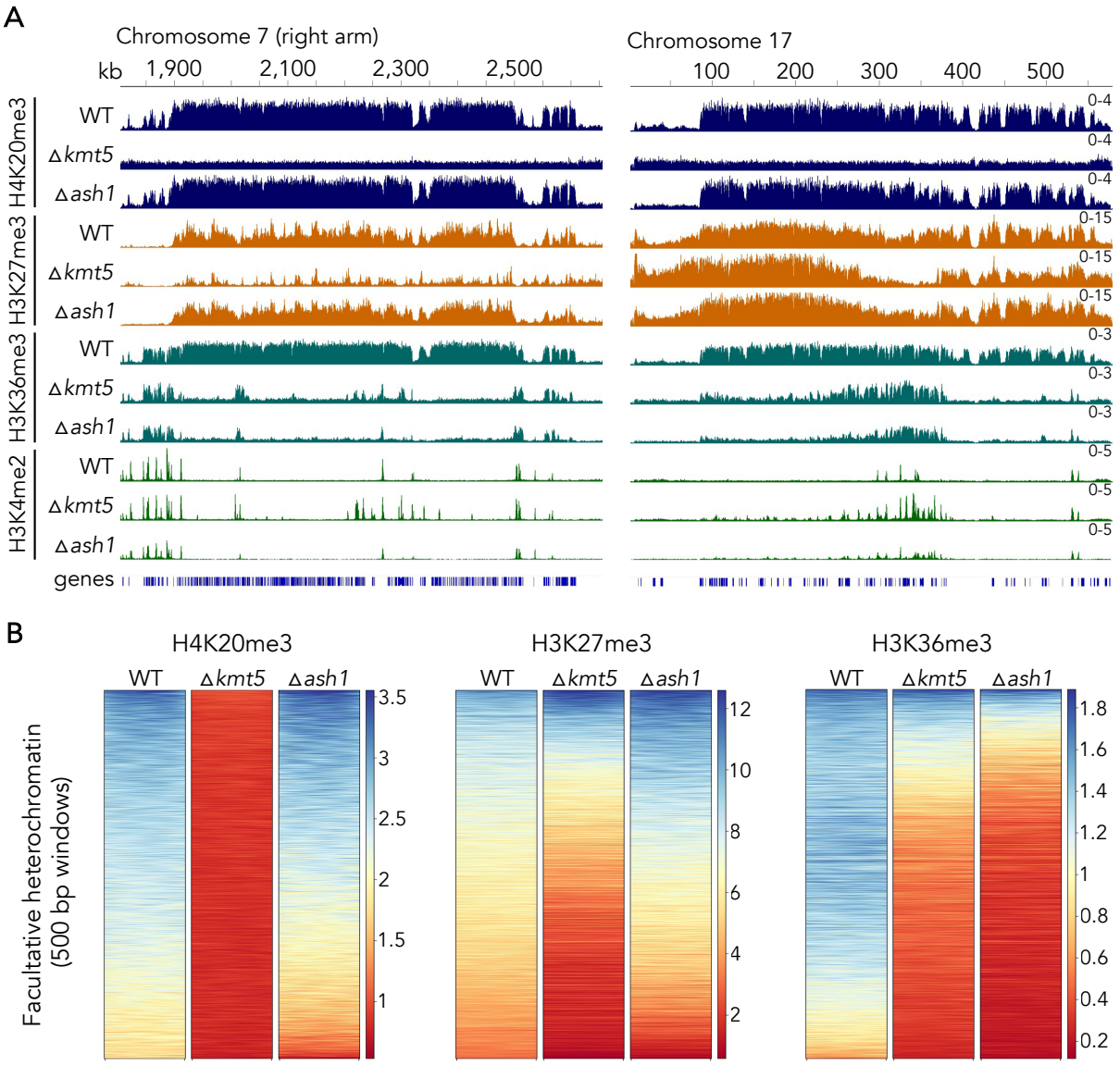

Figure 4: Effects of deletion of *kmt5* or *ash1*, encoding two histone methyltransferases involved in the regulation of H4K20me3 and H3K36me3 levels. A) In the absence of Kmt5, all H4K20 methylation is removed but H4K20me3 enrichment is not affected by lack of Ash1. Lack of Kmt5 or Ash1 alters H3K27me3 in selected regions of the genome, and the lack of either Kmt5 or Ash1 removes H3K36me3 from regions that are not methylated by a second H3K36 methyltransferase, Set2. H3K36 methylation by Set2 is largely correlated with H3K4me2. These results strongly suggest that Kmt5 controls at least some H3K36 methylation, which in turn controls H3K27me3 in some regions of the genome. **B)** Comparison of enrichment of histone modifications in regions of facultative heterochromatin. Deletion of *kmt5* results in loss of H4K20me3, overall reduction in H3K27me3, and strong reduction in H3K36me3. Deletion of *ash1* affects H4K20me3 and H3K27me3 only mildly but strongly reduces H3K36me3 in these regions.

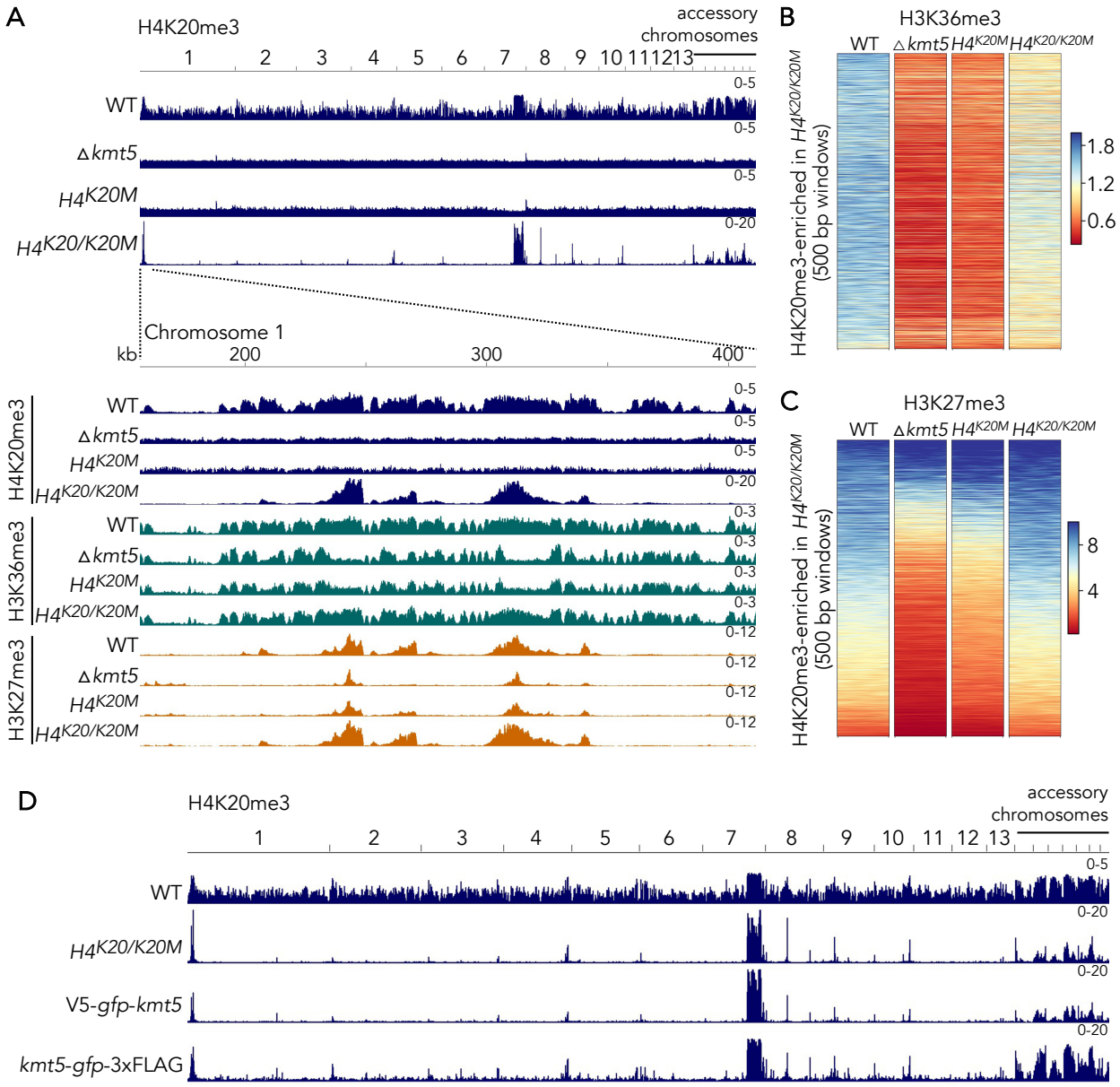

Figure 5: An H4^{K20M} substitution phenocopies deletion of *kmt5* but heterozygous H4$^{K20/K20M}$ strains show specific H4K20me3 in regions of facultative heterochromatin in wild type. A) H4K20me3 distribution in Δ*kmt5* and histone mutants. **B)** and **C)** Effects of deletion of *kmt5* or substitution to H4^{K20M} and H4$^{K20/K20M}$ on regions that retain H4K20me3 in H4$^{K20/K20M}$ strains. **B)** H3K36me3 is severely reduced in Δ*kmt5* and H4^{K20M} but partly restored in H4$^{K20/K20M}$. **C)** H3K27me3 is reduced in *kmt5* and H4^{K20M} but similar to wild-type levels in H4$^{K20/K20M}$. **D)** A similar effect on H4K20me3 observed with heterozygous H4$^{K20/K20M}$ is found when Kmt5 is tagged with GFP on either the amino or carboxy terminus.

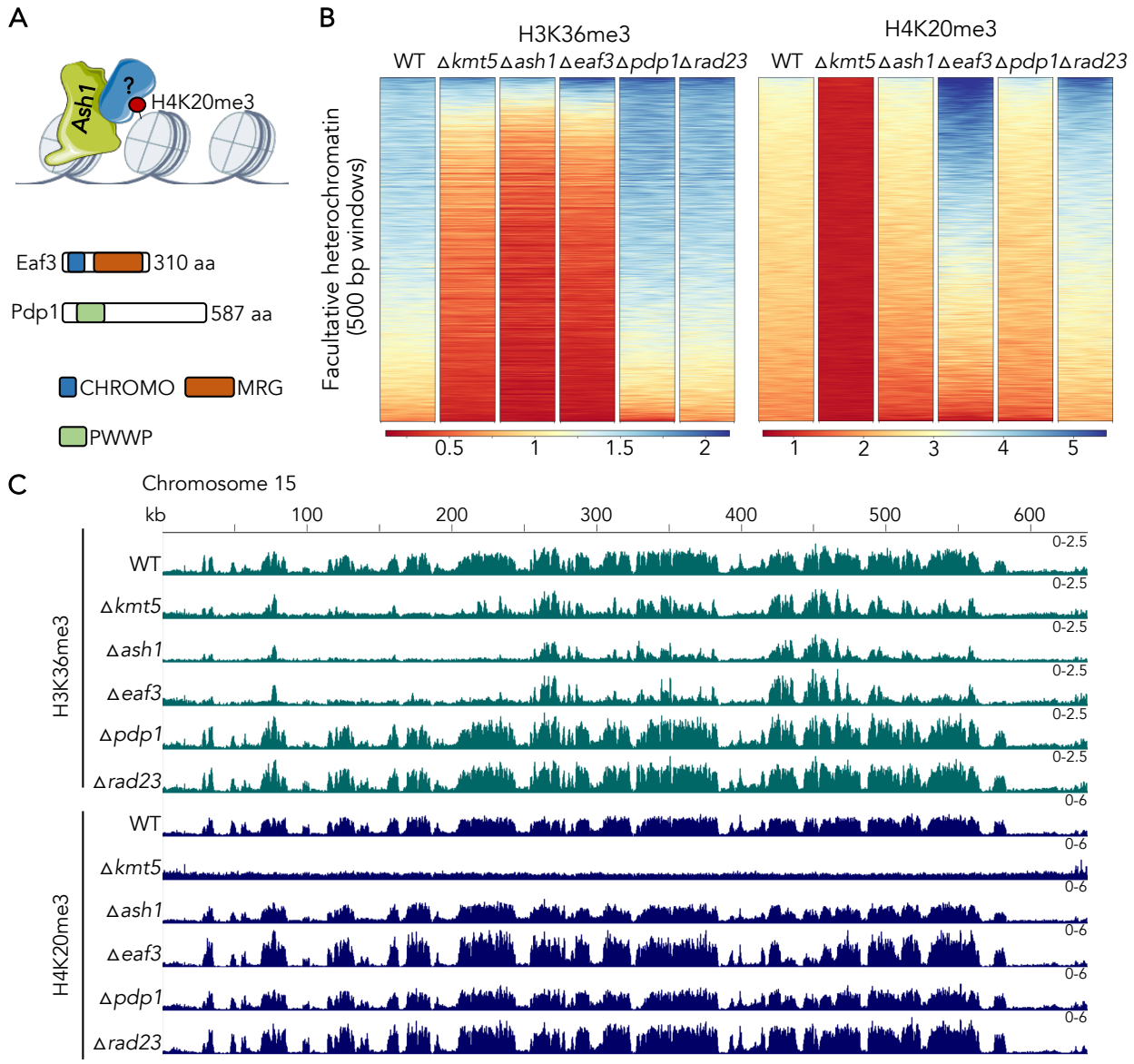

Figure 6: Eaf3 links H4K20 and H3K36 methylation. A) A putative H4K20me3-binding protein ("?") attracts the Ash1 H3K36 methyltransferase, Ash1, to H4K20me3-enriched regions. The PWWP motif protein, Pdp1, is essential for H4K20me in fission yeast, while the CHROMO and MRG domain protein, Eaf3, had been shown to bind H3K36me3 in multiple organisms. **B)** Enrichment of H4K20me3 and H3K36me3 in facultative heterochromatin. We excluded the putative Pdp1 homolog (*pdp1*) because deletion of this gene had no effects on H4K20 or H3K36 methylation when compared to WT. The homologue of Eaf3, however, resulted in a large increase in H4K20me3, and a loss in H3K36me3, suggesting that it may interact with both H4K20me3 and H3K36me3. Loss of the potential H4K20me3 demethylase, Rad23, increased H4K20me3 levels. **C)** ChIP-seq tracks showing H3K36me3 and H4K20me3 on accessory chromosome 15 in WT and Δ*kmt5*, Δ*ash1*, Δ*eaf3*, Δ*pdp1* and Δ*rad23* strains.

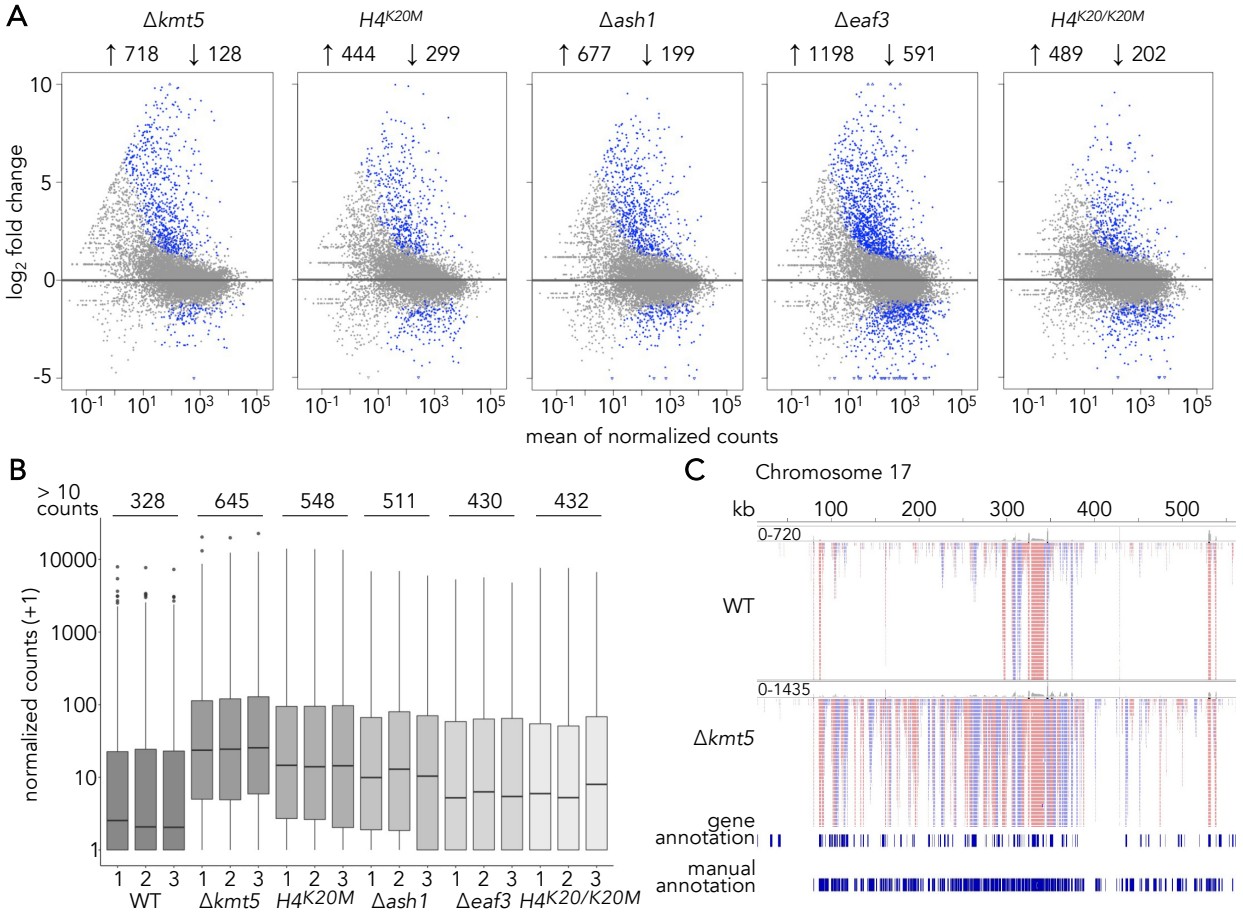

Figure 7: H4K20 methylation is important for transcriptional silencing in facultative heterochromatin. A) Results from differential expression analysis (log2fc > | 0.585 |, *padj* < 0.01) comparing wild-type and mutant strains. **B)** Normalized counts assigned to transcripts in facultative heterochromatin; transcripts were newly annotated with stringtie. RNA-seq results on *kmt5*, *eaf3*, and histone mutants, as well as on wild-type (WT) samples revealed a large group of novel transcripts, especially on accessory chromosomes, that had not been detected before and that come from H3K27me3-enriched regions. These transcripts were more highly expressed in most mutants compared to wild type, especially if H4K20me3 is absent. **C)** RNA-seq reads of wild type and Δ*kmt5* mapped to accessory chromosome 17. The previous annotation (50) identified only a fraction of transcripts expressed on accessory chromosomes.

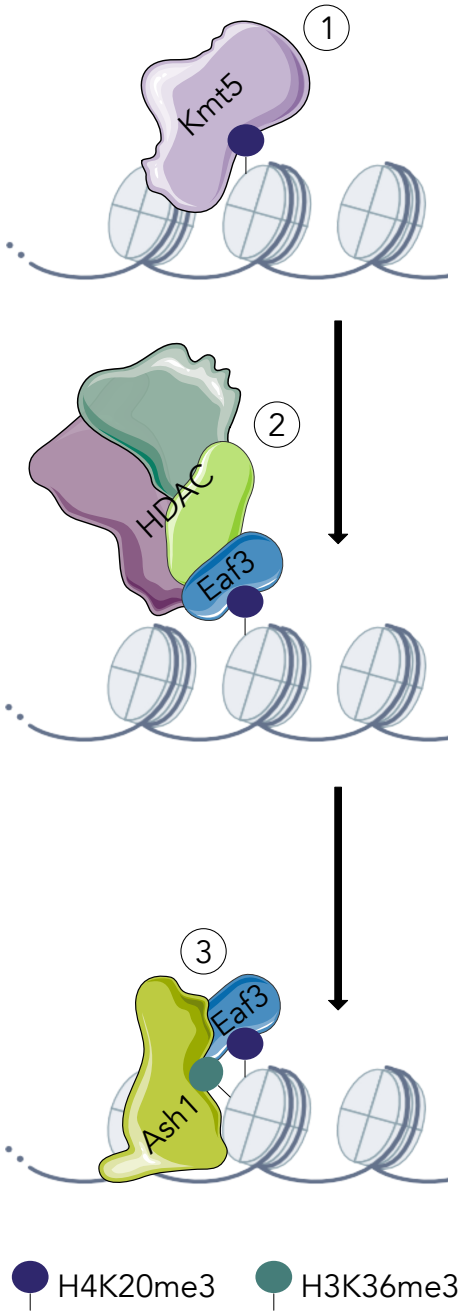

Figure 8: Model of how H4K20me3 is required for Ash1-mediated H3K36me3. (1) Kmt5 mediates H4K20me3 followed by **(2)** binding of Eaf3 to H4K20me3; Eaf3 may be in a complex with a histone deacetylase (e.g., RPD3S). **(3)** Presence of Eaf3 promotes Ash1-mediated H3K36me3.

Supplement

Tables

Table S1. DESeq2 results for all mutants in comparison to wild type including functional annotation.

Table S2. Detailed overview of all manually annotated transcripts on chromosome 17.

Table S3. List of all plasmids, strains and primers generated and used in this study.

Table S4. Summary of all sequencing datasets generated in this study.

Figures

Figure S1. Comparison of H4K20 HMT SET domains. A) Alignment of SET domains of H4K20 methyltransferases in different species. SET domain of human EZH2 is used as an outgroup. B) Phylogenetic tree based on the alignment in A. Numbers indicate substitutions per site. C) Accession numbers of proteins.

Figure S2. Uncropped western blot images for detection of H4K20me1, H4K20me3 and H3.

Figure S3. Southern blots to confirm deletion of *kmt5* and *ash1*. A) Δ*kmt5* mutants show more bands in addition to the expected bands. Because one of the flanks used for homologous recombination and as probe for Southern analyses is a repetitive element, integration into the repetitive element may have altered restriction sites, and additional bands are detected because of TE copy number. Deletion of *kmt5* was confirmed in all ChIP- and RNA-seq datasets. Strains used for further analyses were 95 and 100. B) Confirmation of Δ*ash1*. Strains used for further analyses were 5 and 25.

Figure S4. Phenotypic characterization of WT, Δ*kmt5*, Δ*ash1*, $H4^{K20M}$, $H4^{K20/K20M}$ and Δ*eaf3* under different genotoxic stress conditions and temperatures.

Figure S5. Genome-wide distribution of H4K20me3, H3K36me3, H3K27me3, H3K9me3 and H3K4me2 in wild type.

Figure S6. Interacting genomic regions in the Δ*kmt6* genome. Shown are $\log_2$ ratio of observed interactions relative to expected interactions, fewer interactions than expected are shown in blue, more interactions are shown in red.

Figure S7. Enrichment of different histone marks outside (A) and within (B) facultative heterochromatin regions. While we observed subtle changes outside of facultative

1025 heterochromatin, we observed the most prevalent differences in regions of facultative
1026 heterochromatin.
1027
1028 **Figure S8.** Genome-wide distribution of H4K20me3, H3K36me3 and H3K27me3 in all mutants
1029 generated in this study. There are no ChIP-seq data for H3K36me3 in the tagged Kmt5 strains.
1030
1031 **Figure S9.** ChIP-seq of the Δ*pdp1* revealed an increase in H3K27me3 outside of facultative
1032 heterochromatin regions in WT. A) ChIP-seq tracks (chromosome 10 as an example region) show
1033 that H3K27me3 enrichment increases in gene-dense regions that are also enriched with
1034 H4K20me3 and H3K36me3 but not H3K9me3. B) H3K27me3 levels decrease in facultative
1035 heterochromatin but increase in some non-facultative heterochromatin regions.
1036
1037 **Figure S10.** RNA sequencing of mutant strains. A) Principal Component Analysis (PCA) plot of all
1038 sequenced replicate strains. B) Venn diagram of upregulated genes in all mutants compared to
1039 wild type.
1040
1041 *Methods*
1042
1043 ChIP analysis
1044 RNA-seq analysis
1045 Hi-C analysis
1046
1047 ChIP protocol
1048 Stranded mRNA library protocol
1049 Modified NEB Illumina library protocol
1050 *Zymoseptoria* transformation protocol

A

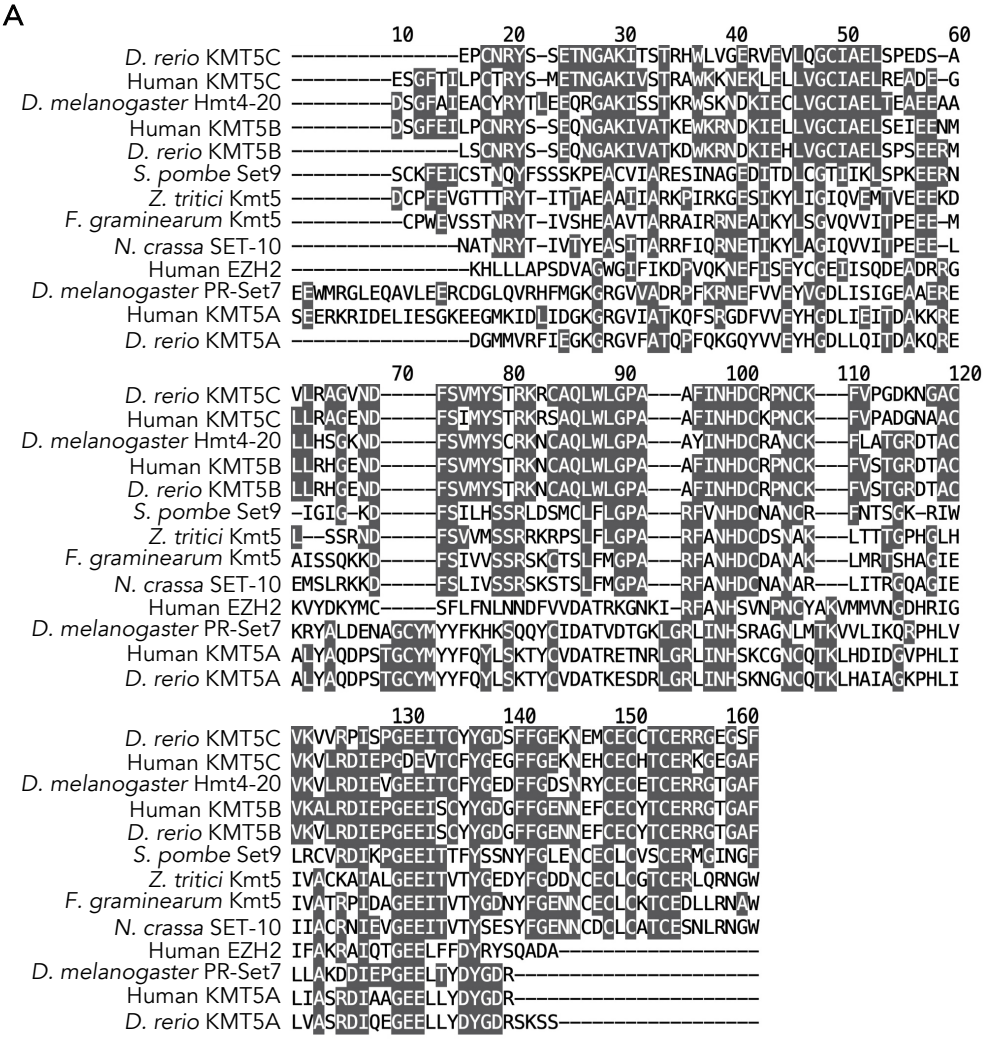

B

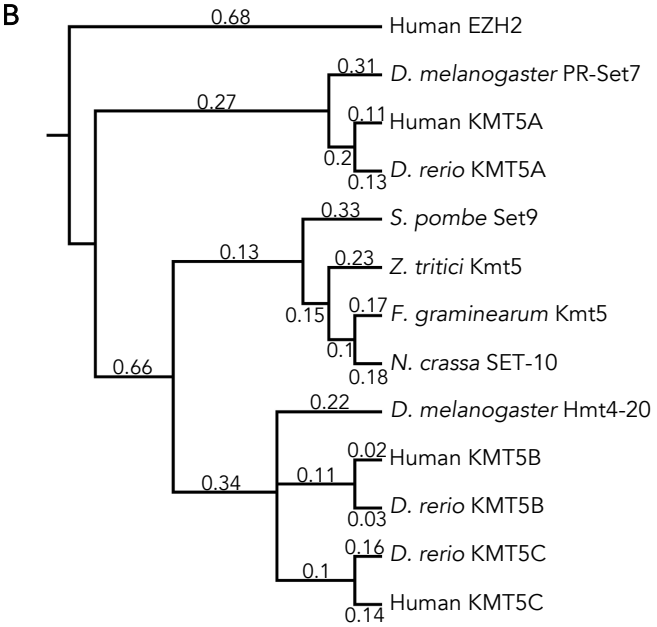

C

Protein	Accession
Human EZH2	XP_005250019.1
D. melanogaster PR-Set7	NP_001247100.1
Human KMT5A	Q9NQR1.3
D. rerio KMT5A	NP_001038814.2
S. pombe Set9	NP_588078.1
Z. tritici Kmt5	SMQ48785.1
F. graminearum Kmt5	XP_011326140.1
N. crassa SET-10	XP_963033.2
D. melanogaster Hmt4-20	NP_569853.1
Human KMT5B	NP_001356355.1
D. rerio KMT5B	Q5U3H2.2
D. rerio KMT5C	NP_001091656.1
Human KMT5C	NP_116090.2

1052 **Figure S1.** Comparison of H4K20 HMT SET domains. A) Alignment of SET domains of H4K20
1053 methyltransferases in different species. SET domain of human EZH2 is used as an outgroup. B)
1054 Phylogenetic tree based on the alignment in A. Numbers indicate substitutions per site. C)
1055 Accession numbers of proteins.

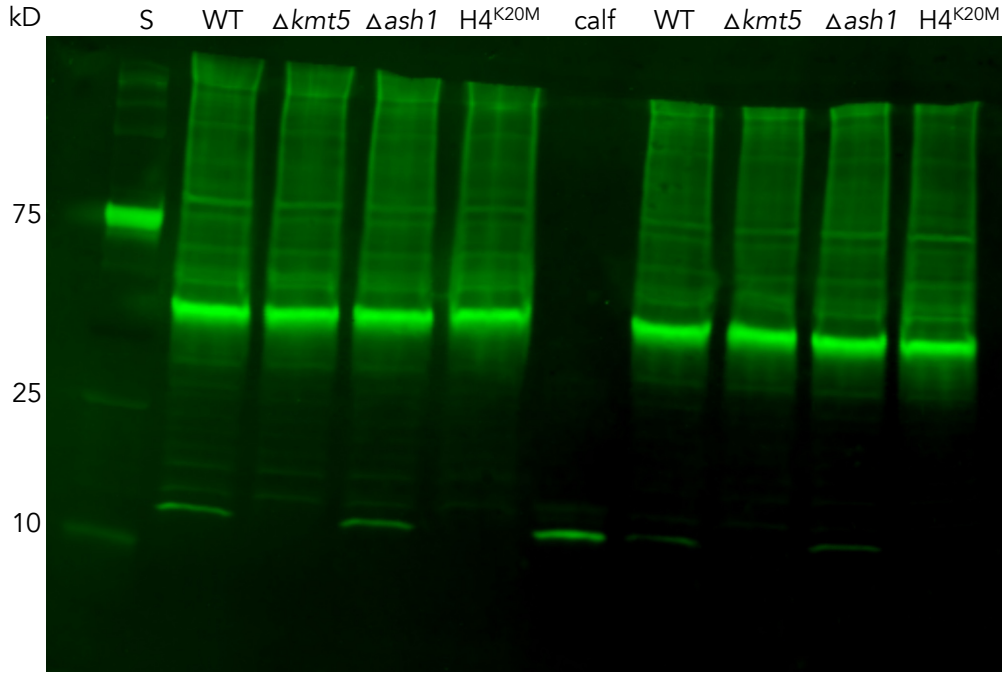

αH4K20me3 (Active motif 39180, pAb, anti-rabbit, green) 1:2000
IRDye 800CW Goat anti-Rabbit IgG (LI-COR 926-32211) 1:5000
Standard: BioRad precision plus protein kaleidoscope pre-stained protein

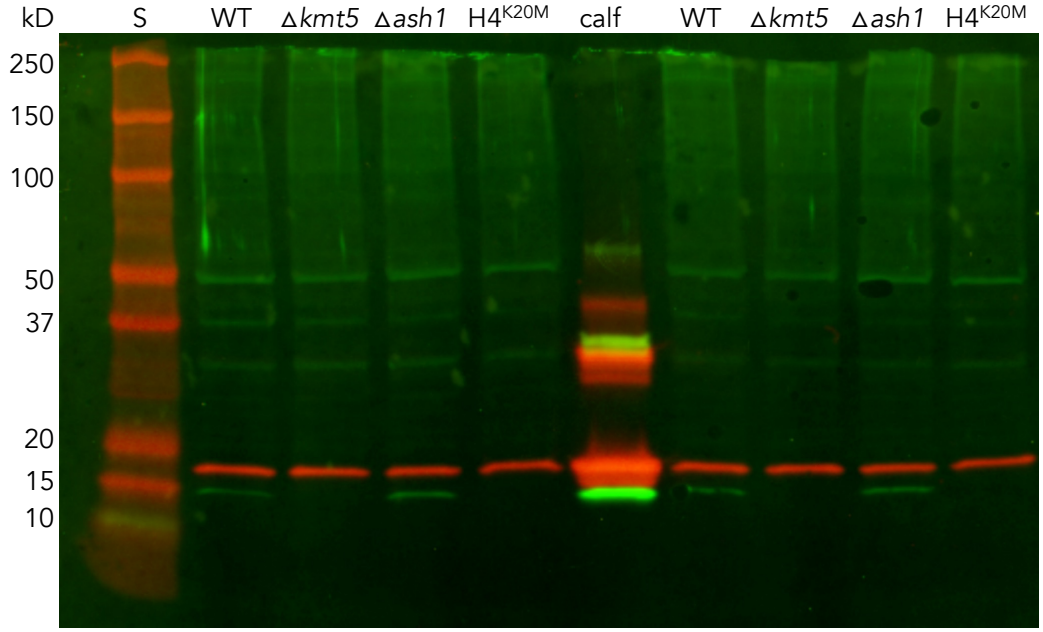

αH3 (Active motif 39763, mAb, anti-mouse, red) 1:5000
αH4K20me1 (abcam 9051, pAb, anti-rabbit, green) 1:1000
IRDye 680RD Goat anti-Mouse IgG (LI-COR 926-68070) 1:5000
IRDye 800CW Goat anti-Rabbit IgG (LI-COR 926-32211) 1:5000
Standard: BioRad precision plus protein kaleidoscope pre-stained protein

Figure S2. Uncropped western blots for detection of H4K20me1, H4K20me3 and H3.

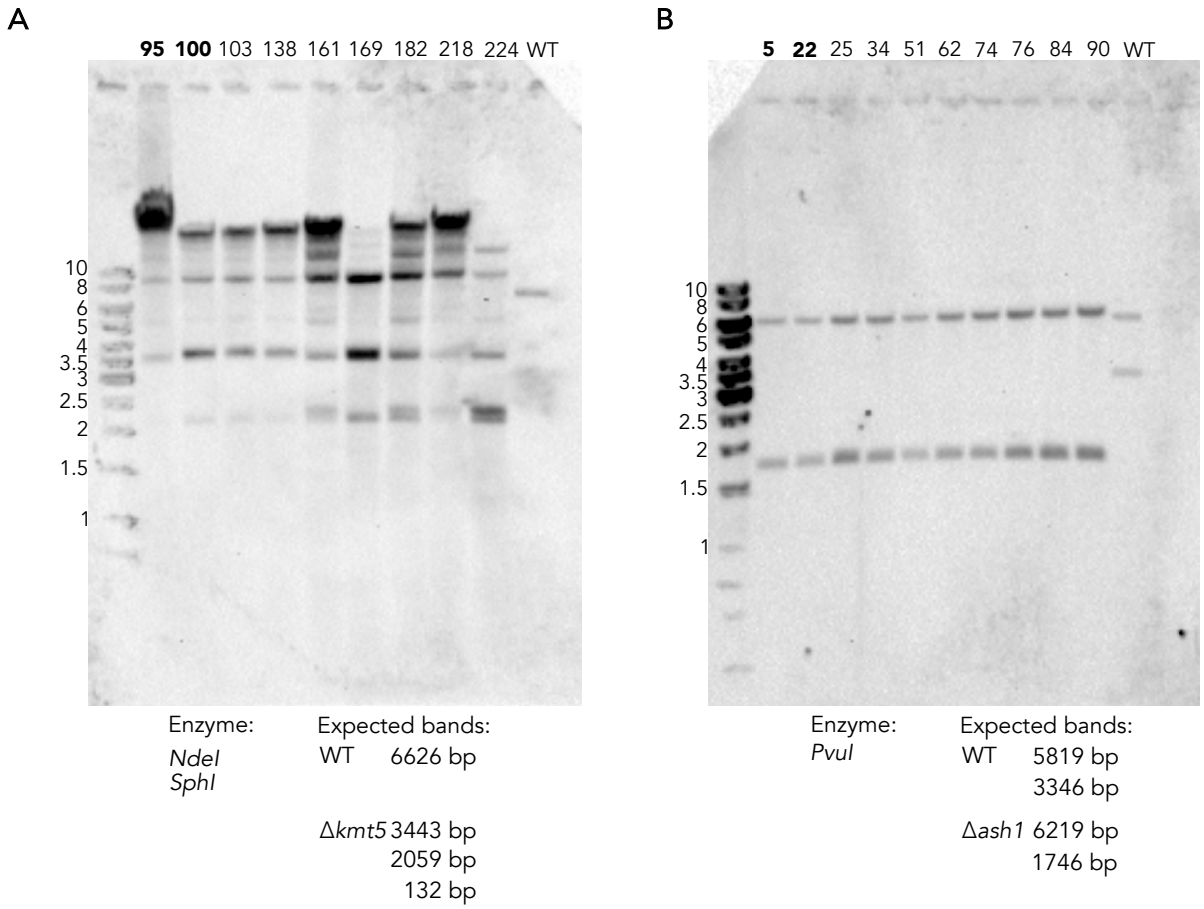

Figure S3. Southern blots to confirm deletion of *kmt5* and *ash1*. A) Δ*kmt5* mutants show more bands in addition to the expected bands. Because one of the flanks used for homologous recombination and as probe for Southern analyses is a repetitive element, integration into the repetitive element may have altered restriction sites, and additional bands are detected because of TE copy number. Deletion of *kmt5* was confirmed in all ChIP- and RNA-seq datasets. Strains used for further analyses were 95 and 100. B) Confirmation of Δ*ash1*. Strains used for further analyses were 5 and 25.

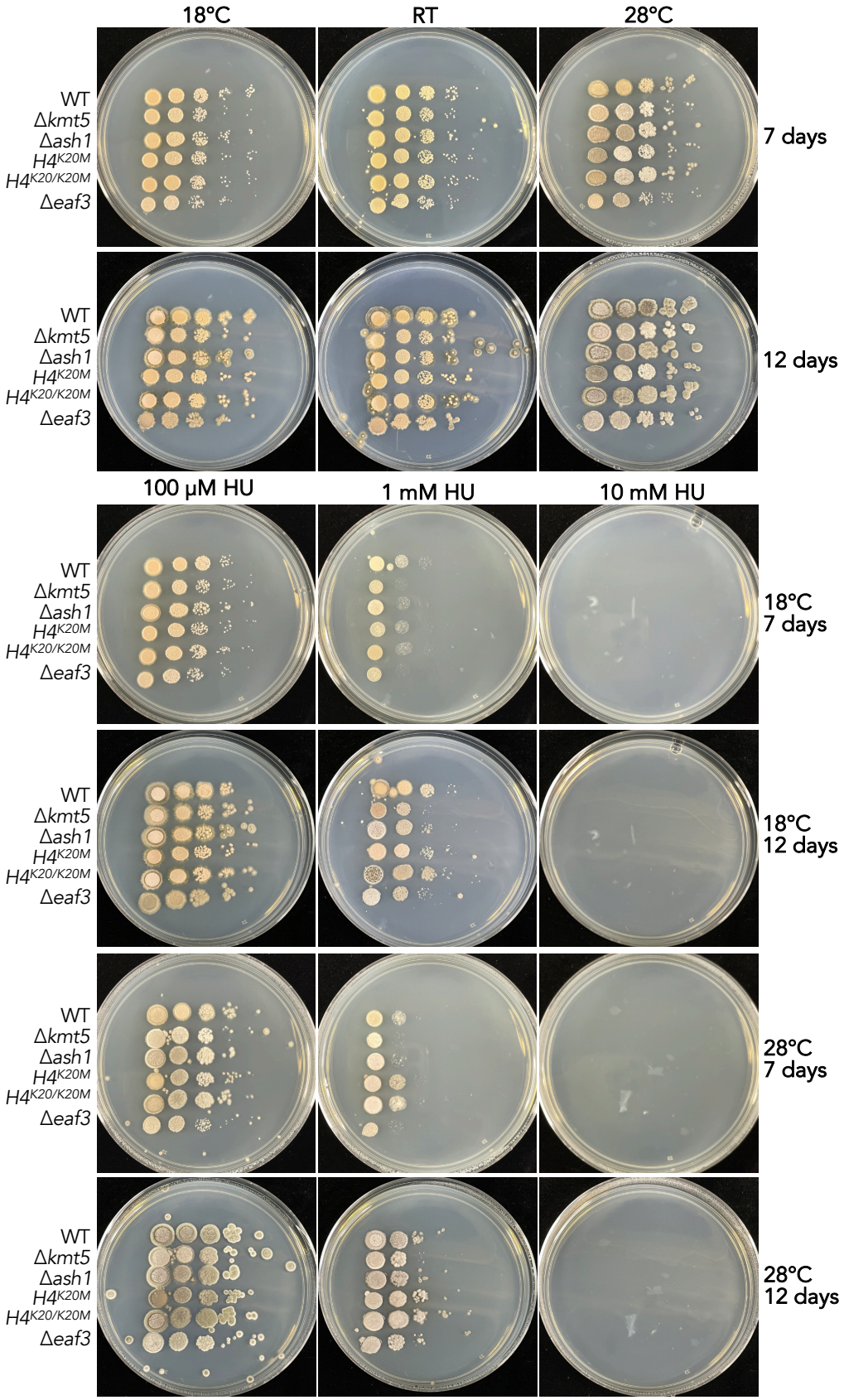
18°C
RT
28°C
WT
Δkmt5
Δash1
H4K20M
H4K20/K20M
Δeaf3
7 days
12 days
100 μM HU
1 mM HU
10 mM HU
18°C
7 days
18°C
12 days
28°C
7 days
28°C
12 days

1065

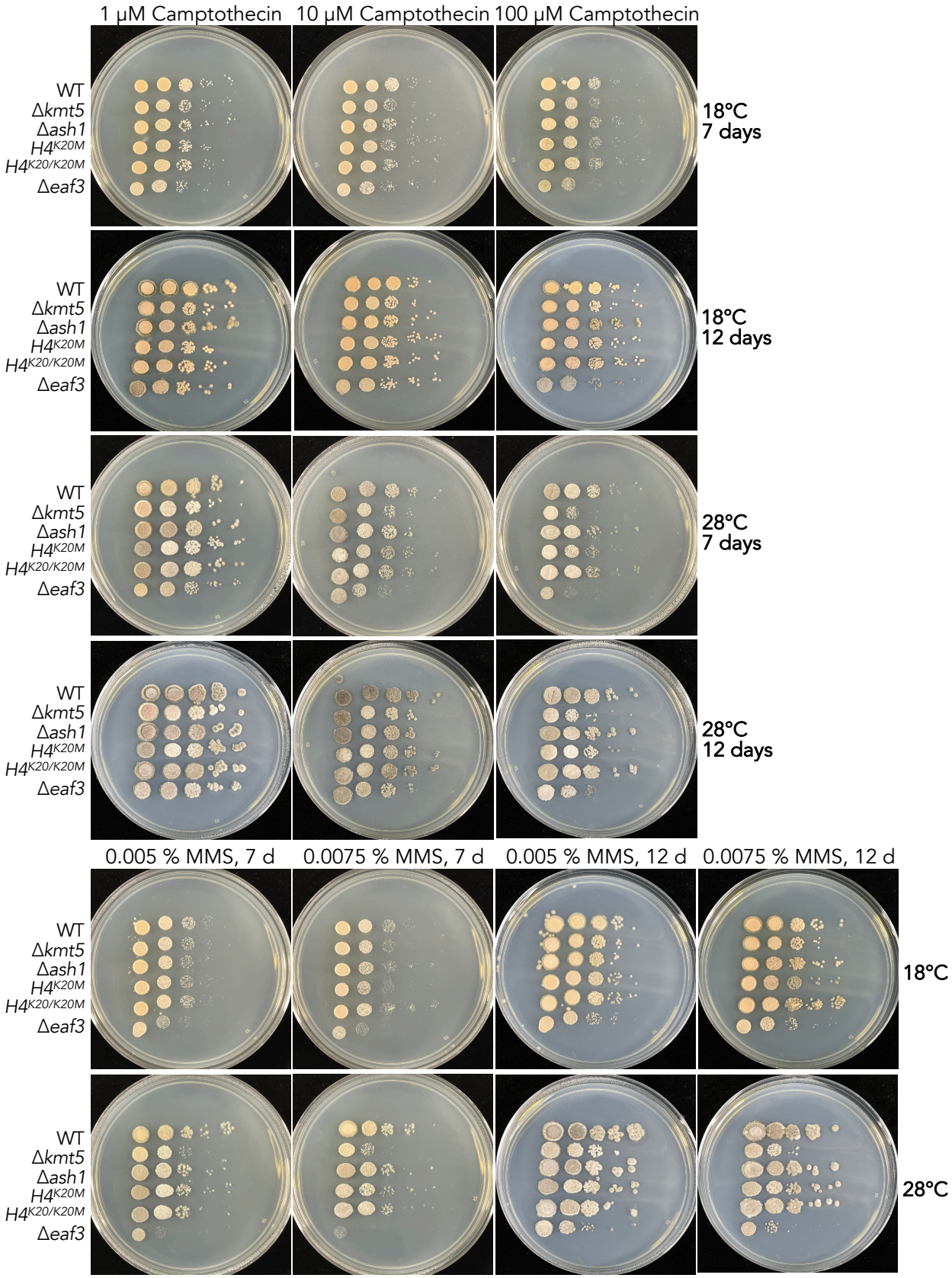
1 μM Camptothecin
10 μM Camptothecin
100 μM Camptothecin
WT
Δkmt5
Δash1
H4K20M
H4K20/K20M
Δeaf3
18°C
7 days
18°C
12 days
28°C
7 days
28°C
12 days
0.005 % MMS, 7 d
0.0075 % MMS, 7 d
0.005 % MMS, 12 d
0.0075 % MMS, 12 d
18°C
28°C

1066

1067 **Figure S4.** Phenotypic characterization of WT, Δ*kmt5*, Δ*ash1*, *H4*^{K20M}, H4$^{K20/K20M}$ and Δ*eaf3* under
1068 different genotoxic stress conditions and temperatures.

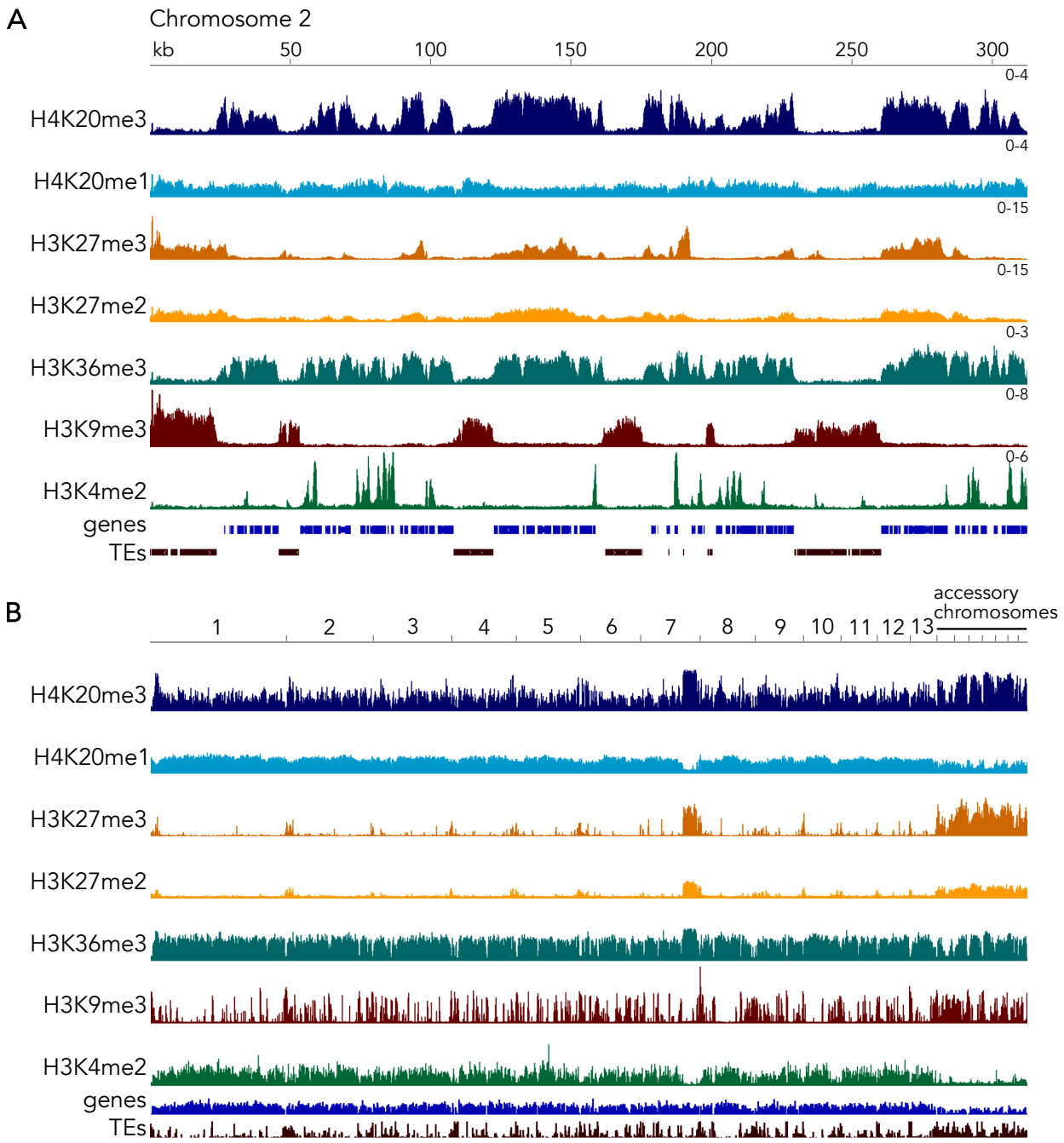

Figure S5. Genome-wide distribution of H4K20me3, H3K36me3, H3K27me3, H3K9me3 and H3K4me2 in wild type.

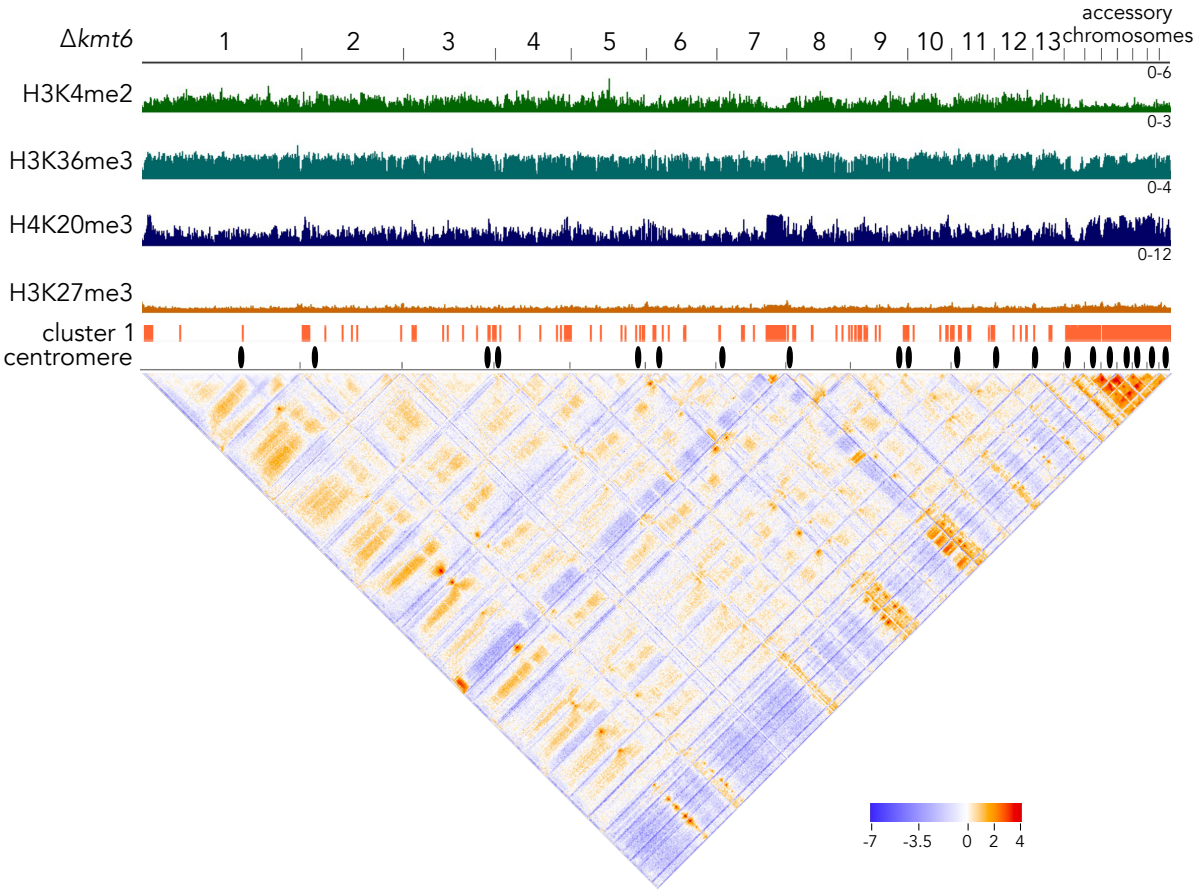

Figure S6. Interacting genomic regions in the Δ*kmt6* genome. Shown are $\log_2$ ratio of observed interactions relative to expected interactions, fewer interactions than expected are shown in blue, more interactions are shown in red.

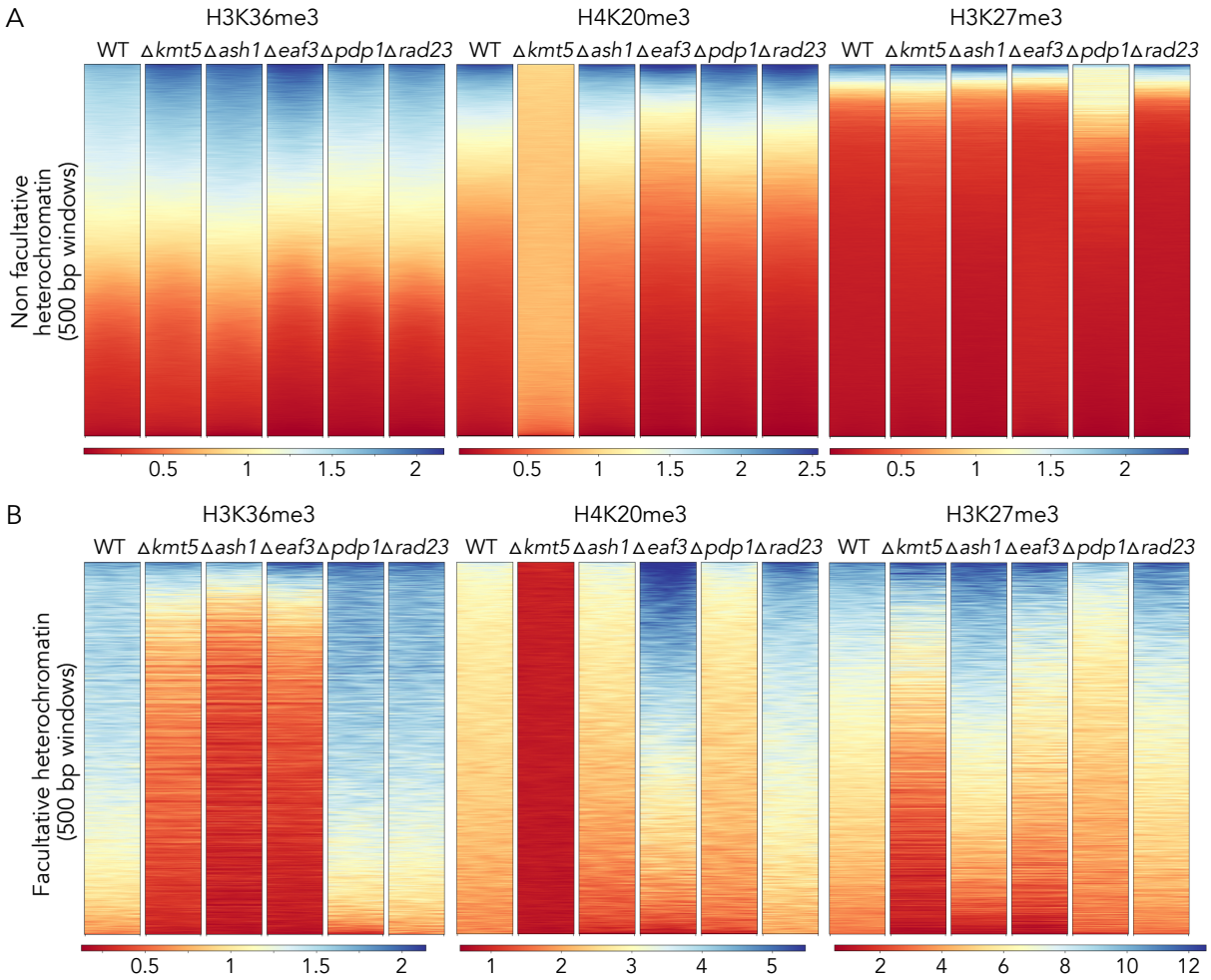

Figure S7. Enrichment of different histone marks outside (A) and within (B) facultative heterochromatin regions. While we observed subtle changes outside of facultative heterochromatin, we observed the most prevalent differences in regions of facultative heterochromatin.

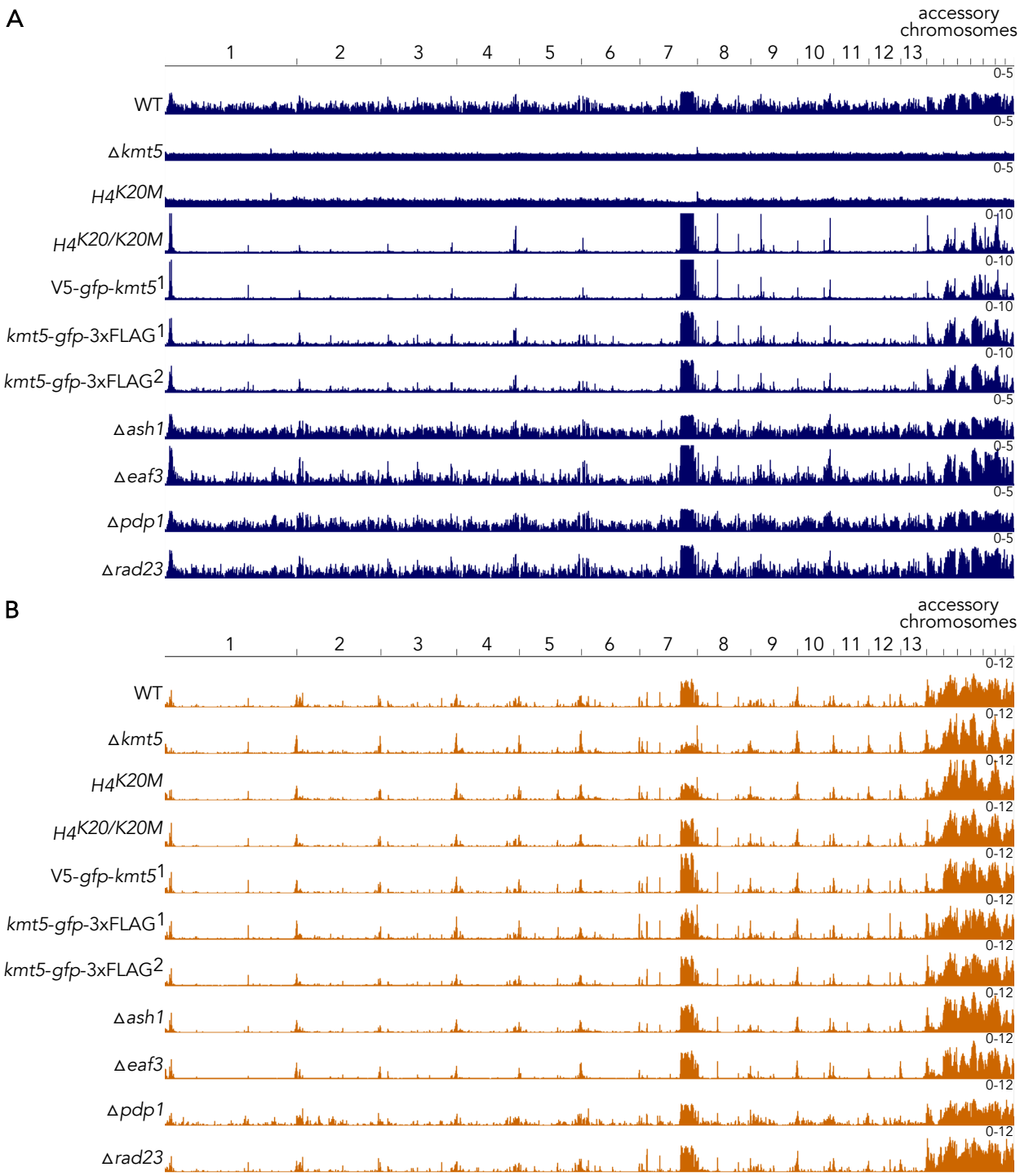
A
accessory chromosomes
1 2 3 4 5 6 7 8 9 10 11 12 13
WT
Δkmt5
H4K20M
H4K20/K20M
V5-gfp-kmt5 1
kmt5-gfp-3xFLAG 1
kmt5-gfp-3xFLAG 2
Δash1
Δeaf3
Δpdp1
Δrad23
0-5
0-10
B
accessory chromosomes
1 2 3 4 5 6 7 8 9 10 11 12 13
0-12

1081

1082

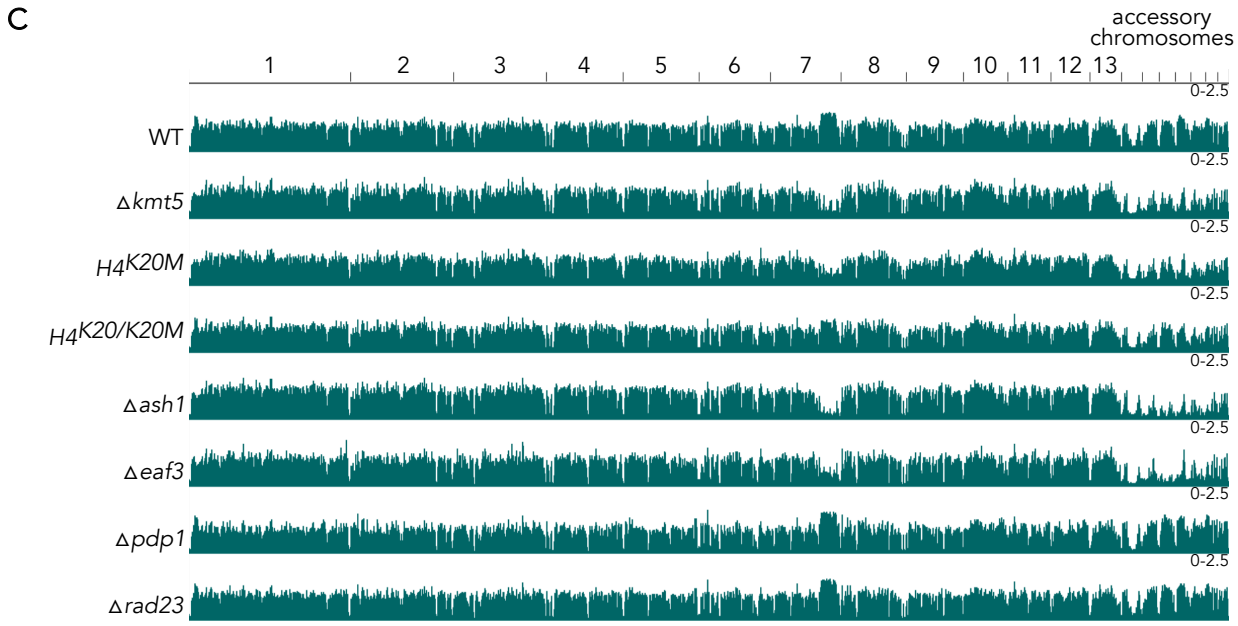

1083 **Figure S8.** Genome-wide distribution of H4K20me3, H3K36me3 and H3K27me3 in all mutants
1084 generated in this study. There are no ChIP-seq data for H3K36me3 in the tagged Kmt5 strains.

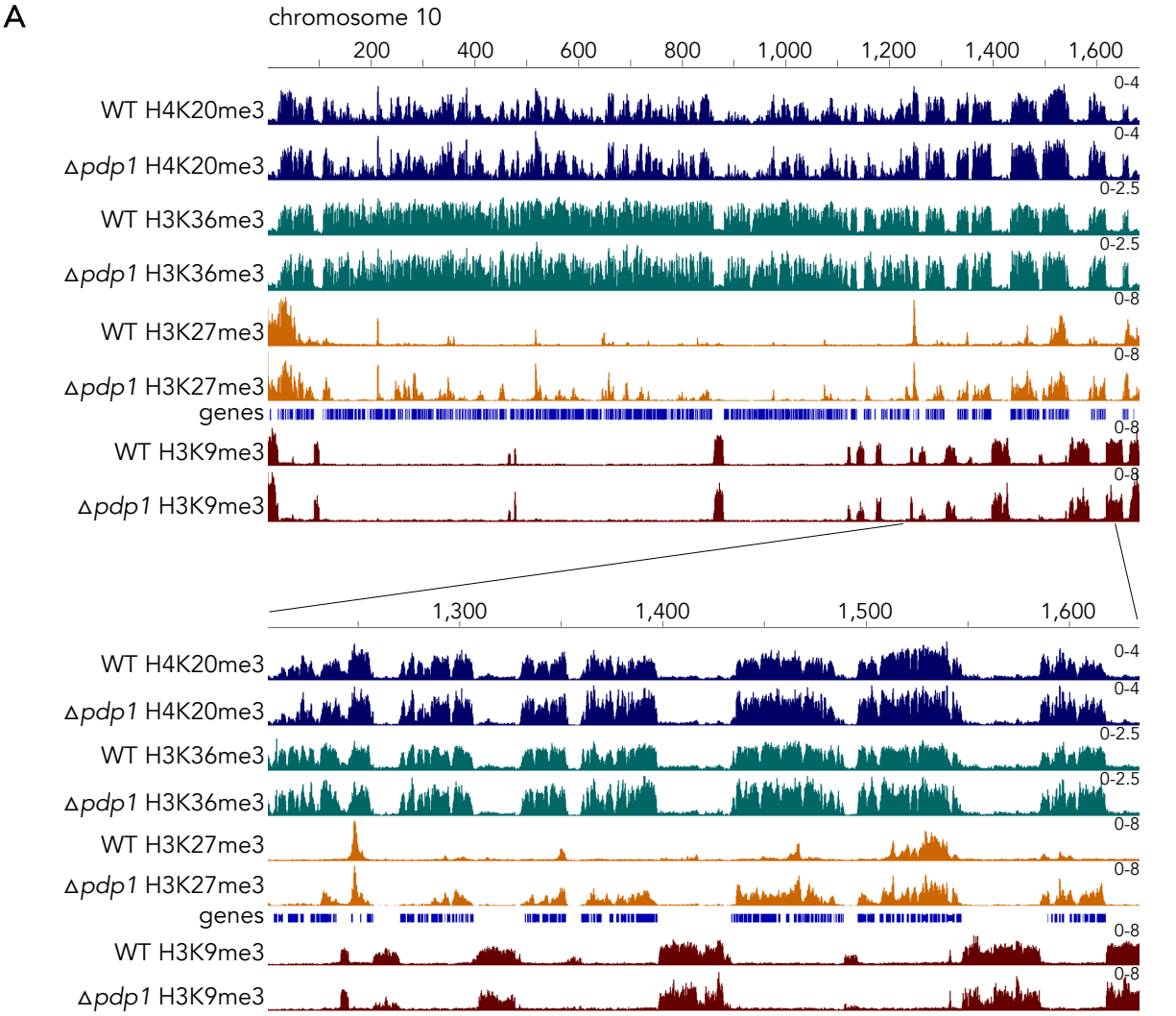
A
chromosome 10
200
400
600
800
1,000
1,200
1,400
1,600
WT H4K20me3
Δpdp1 H4K20me3
WT H3K36me3
Δpdp1 H3K36me3
WT H3K27me3
Δpdp1 H3K27me3
genes
WT H3K9me3
Δpdp1 H3K9me3
0-4
0-2.5
0-8
1,300
1,400
1,500
1,600

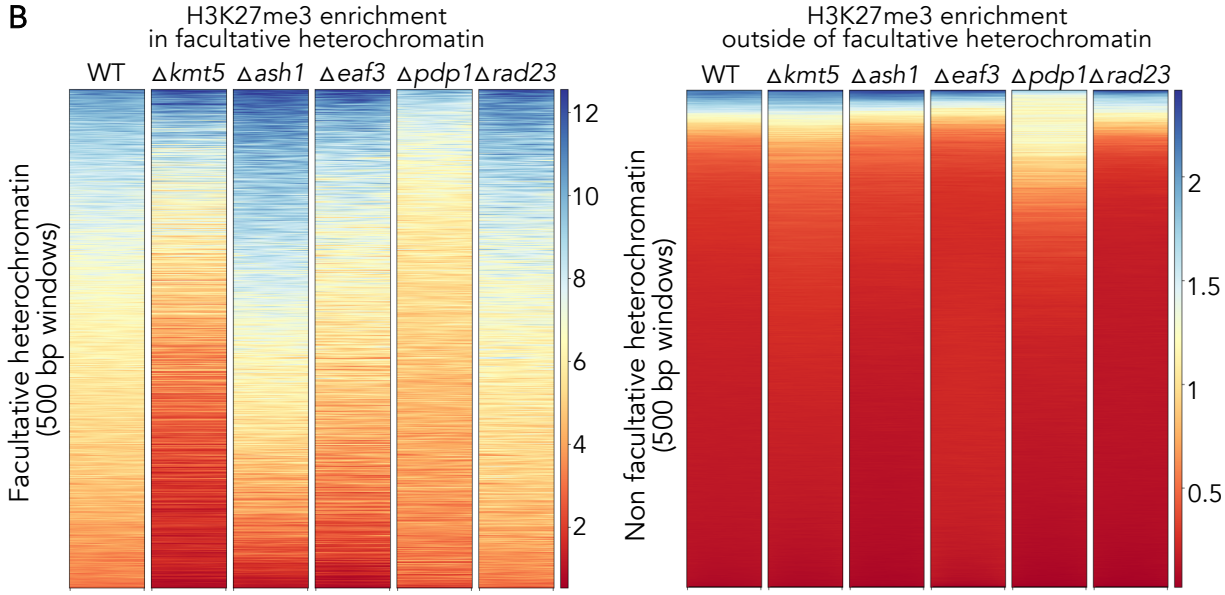
B
H3K27me3 enrichment
in facultative heterochromatin
WT
Δkmt5
Δash1
Δeaf3
Δpdp1Δrad23
Facultative heterochromatin
(500 bp windows)
12
10
8
6
4
2
H3K27me3 enrichment
outside of facultative heterochromatin
Non facultative heterochromatin
(500 bp windows)
2
1.5
1
0.5

1085

1086 **Figure S9.** ChIP-seq of the Δ*pdp1* revealed an increase in H3K27me3 outside of facultative
1087 heterochromatin regions in WT. A) ChIP-seq tracks (chromosome 10 as an example region) show
1088 that H3K27me3 enrichment increases in gene-dense regions that are also enriched with
1089 H4K20me3 and H3K36me3 but not H3K9me3. B) H3K27me3 levels decrease in facultative
1090 heterochromatin but increase in some non-facultative heterochromatin regions.

A

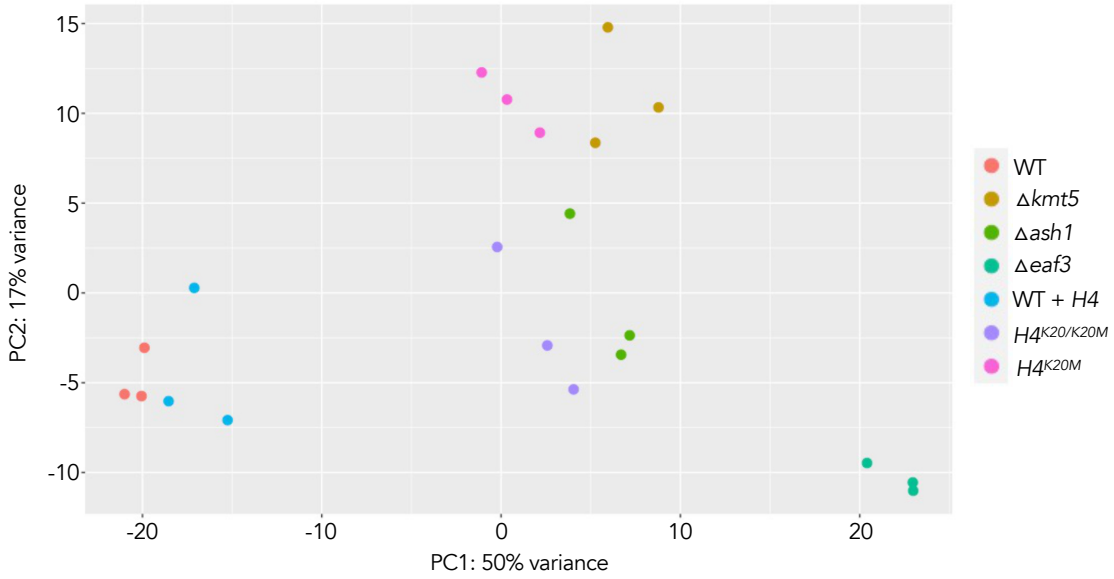
15
10
5
0
-5
-10
PC2: 17% variance
-20
-10
0
10
20
PC1: 50% variance
WT
Δkmt5
Δash1
Δeaf3
WT + H4
H4K20/K20M
H4K20M

B

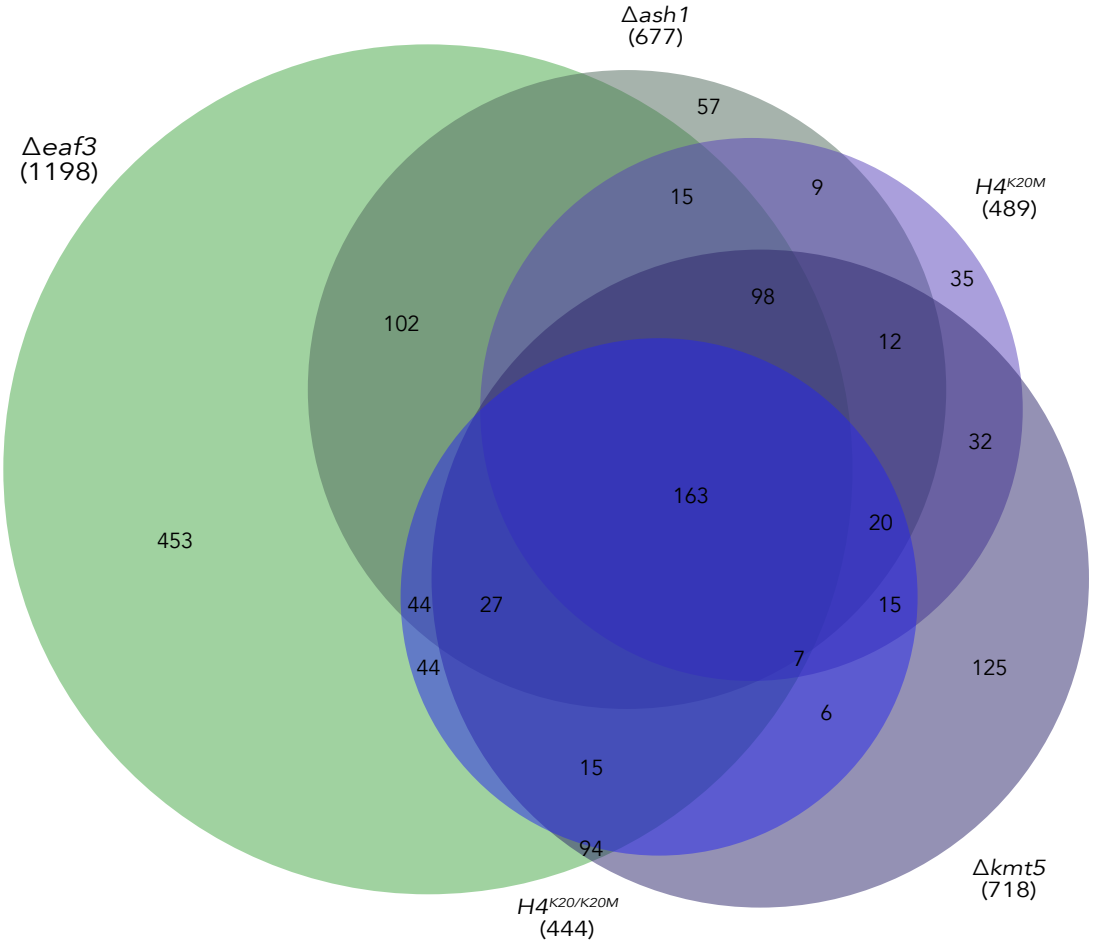
Δash1
(677)
Δeaf3
(1198)
H4K20M
(489)
Δkmt5
(718)
H4K20/K20M
(444)
57
15
9
35
98
102
12
32
163
20
453
44
27
15
44
7
125
6
15
94

1091

1092 **Figure S10.** RNA sequencing of mutant strains. A) Principal Component Analysis (PCA) plot of all
1093 sequenced replicate strains. B) Venn diagram of upregulated genes in all mutants compared to
1094 WT.